SCIEPublish

Review

Application of Polydopamine-Based Photocatalysts in Energy and Environmental Systems

Hui Wang [1], Liquan Jing [1,*], Amir Varamesh [1], Yubo Yan [1,2], Hongguang Zhang [1], Qi Gao [1] and Jinguang Hu [1,*]

[1] Department of Chemical and Petroleum Engineering, University of Calgary, 2500 University Drive, NW, Calgary, AB T2N1N4, Canada; hui.wang6@ucalgary.ca (H.W.); amir.varamesh@ucalgary.ca (A.V.); yubo.yan@hytc.edu.cn (Y.Y.); hongguang.zhang@ucalgary.ca (H.Z.); qi.gao2@ucalgary.ca (Q.G.)

[2] School of Chemistry and Chemical Engineering, Huaiyin Normal University, Huai'an 223300, China

* Corresponding author. E-mail: liquan.jing@ucalgary.ca (L.J.); jinguang.hu@ucalgary.ca (J.H.)

Received: 29 July 2024; Accepted: 4 September 2024; Available online: 9 September 2024

ABSTRACT: Polydopamine (PDA) is also widely sought after in photocatalytic applications due to its fascinating properties such as simple preparation, templating agent, near-infrared absorption, high photothermal conversion efficiency, abundant functional groups, and strong chelating effect of metal ions. This review will present the structural features and synthetic methods of PDA, the advantages of PDA for photocatalytic applications (templating agent effect, light absorption properties, film-forming properties, hydrophilicity, conductivity, etc.), the modulation strategies of PDA for photocatalytic applications, and the use of PDA-based photocatalytic materials for solar-powered water purification (heavy metal adsorption and reduction, catalytic degradation of organic pollutants, and antimicrobial properties), hydrogen production, hydrogen peroxide production, CO_2 reduction, and organic conversion. Finally, this review will provide valuable information for the design and development of PDA-based photocatalytic materials.

Keywords: Polydopamine; Photocatalyst; Energy; Environment

1. Introduction

Photocatalytic technology has important applications, especially in the fields of environmental remediation, energy conversion, and synthetic chemistry, by using light energy to excite semiconductor materials to generate electron and hole pairs and initiate chemical reactions [1–4]. The photocatalytic process involves light absorption, separation and migration of electron-hole pairs, and reaction with molecules at the material surface [5]. Despite the challenges of limited light absorption range, and material stability, high photogenerated carrier complexity, the development of new materials will promote its application in the environmental and energy fields [6,7].

Polydopamine (PDA), as an emerging material, has gained much attention in photocatalysis in recent years. Further, PDA exhibited great potential in the field of photocatalysis as a melanoidin-like material with structural diversity (rich functional groups such as phenolic hydroxyl, amino, and amide groups), biocompatibility, good adhesion (stable coating and film-forming properties), and broad-spectrum absorption (capable of absorbing ultraviolet, visible, and near-infrared light) [8,9]. Currently, PDAs have the potential to be used in the effective degradation of organic pollutants, decomposition of water to produce hydrogen, and reduction of carbon dioxide, etc. To improve its photocatalytic performance, researchers have mainly used the strategy of constructing heterojunctions to modulate the electronic structure of PDA and enhance the separation efficiency of photogenerated carriers [10–13]. However, PDA also has drawbacks such as photocorrosion and structural instability, especially in strong acid or alkali environments. In addition, the poor dispersion of PDA nanoparticles will affect the modification of the photocatalyst and reduce the catalytic efficiency [14,15]. Despite some challenges, the continuous optimization and design of PDA makes it a promising prospect for applications in the fields of environmental pollution control, clean energy conversion, and green chemical synthesis. Future research will focus on enhancing their efficiency and stability for a wider range of applications.

https://doi.org/10.70322/prp.2024.10007

In recent years, the preparation and extensive applications of PDA-based materials on photocatalytic have rapidly developed, as shown by the growing publications over past 10 years (Figure 1a). As impressive as the volume of publications on photocatalysis is its broad interdisciplinary contribution. An analysis of the same dataset of photocatalysis publications by discipline revealed that nearly 75% of the research focused in the fields of water purification and water splitting. In addition to that, significant contributions came from CO_2 reduction and H_2O_2 production (Figure 1b).

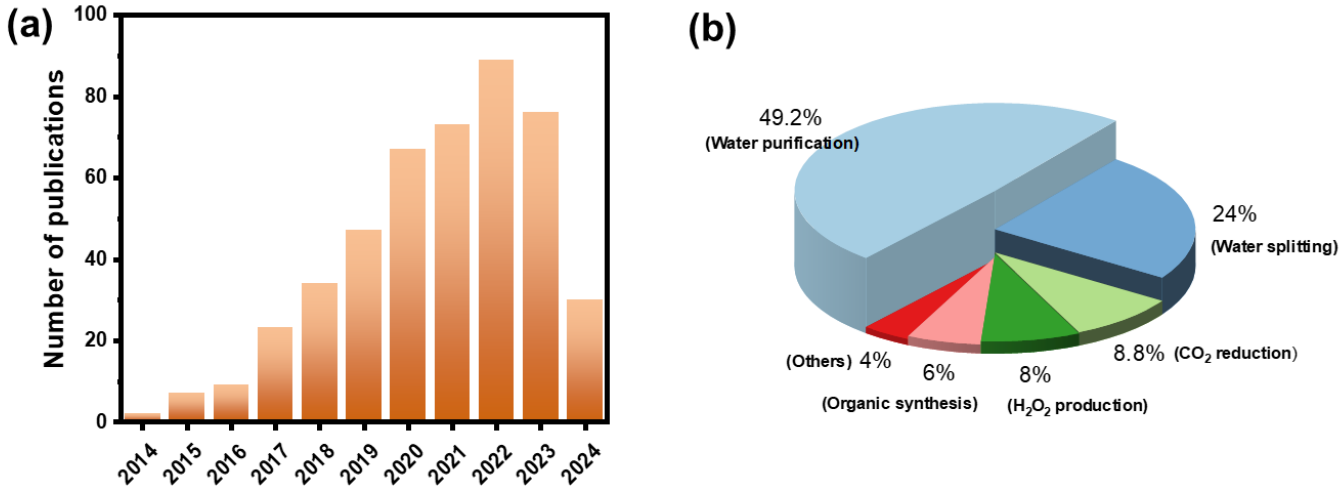

Figure 1. (**a**) Number of publications on PDA-based photocatalysts during the past 10 years (source: Web of Science; date: 30 July. 2024; keywords: polydopamine photocatalytic). (**b**) Pie chart of "PDA-based photocatalysts" by different research areas using the same data as in application.

2. Molecular Structure and Polymerization Mechanisms of PDA

PDA (Polydopamine) is a synthetic polymer inspired by the adhesive proteins found in mussels. Its structure and polymerization process are of significant interest due to its adhesive properties and biocompatibility. The specific process includes dissolving dopamine hydrochloride in a Tris-HCl buffer solution, usually at a pH of 8.5. The solution is stirred at room temperature, allowing the dopamine to undergo self-oxidation in the presence of oxygen in the air, gradually forming polydopamine [16,17]. In PDA, dopamine functions as a building block, consisting of an amine group (a primary amine attached to an ethyl chain) and a catechol group (an ethyl ring). The multiple chemical reaction sites in PDA, complex redox processes, and generates numerous intermediates, resulting in a diverse synthesis mechanism with no definitive conclusion yet. Lee et al. proposed two polymerization mechanisms for PDA: non-covalent self-assembly and covalent polymerization, which have been widely accepted [8,18]. In the covalent reaction pathway, dopamine is first oxidized to a quinone structure. The quinone structure may then be further oxidized to form 5,6-dihydroxyindole (DHI) (Figure 2a), or undergo intermolecular reactions through catechol-catechol coupling. Finally, cross-linking reactions between these intermediates occur, forming the final PDA structure. In addition to covalent polymerization, the formation of PDA also involves a non-covalent self-assembly pathway [19]. As illustrated in Figure 2b, PDA is considered to be an aggregate of monomers that are primarily cross-linked through strong intrachain and interchain non-covalent forces, encompassing hydrogen bonding, charge transfer and π-π stacking, which is similar to other synthetic or biological supramolecular polymers [8,17].

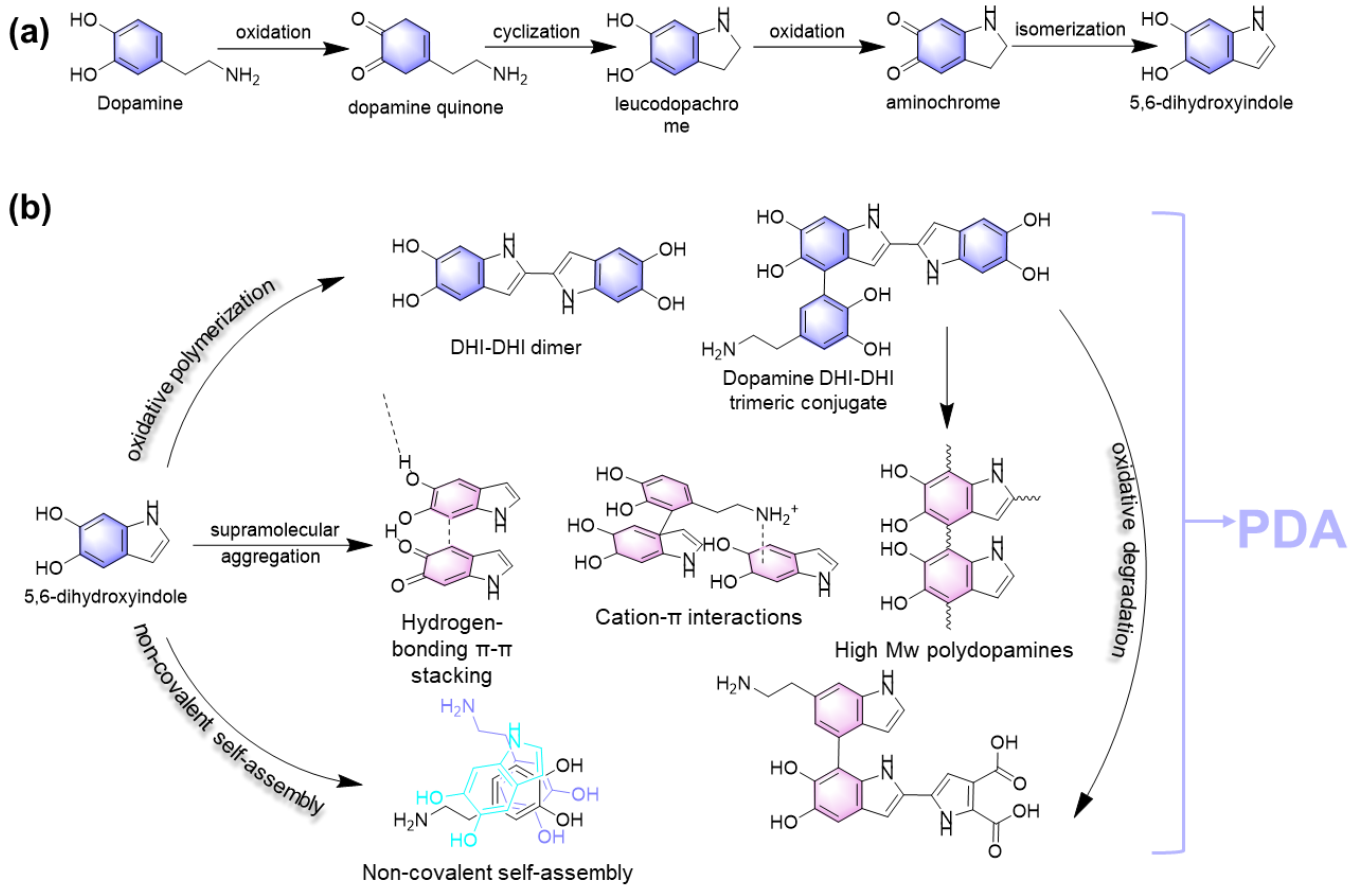

Figure 2. (**a**). Dopamine oxidation and subsequent cyclization and rearrangement; (**b**) The different pathways of PDA formation.

3. Advantages of PDA in the Field of Photocatalysis

3.1. Light Absorption and Excellent Photothermal Conversion Properties

PDA, a black polymer generated through the self-assembly of dopamine, exhibits an expansive light absorption spectrum that spans from the ultraviolet to the near-infrared spectrum. This broad absorption capability stems from the intricate conjugated system within its molecular structure, which consists of aromatic rings intertwined with nitrogen-containing moieties. Additionally, the synergistic conjugation of phenolic hydroxyl and amino groups further facilitates electron transition at diminished energy levels [17]. The optical absorption ability could be boosted by changing the bandgap of PDA, for widely using in photothermal conversion and energy harvesting applications. As reported by Zou et al., doping TEMPO moiety into the PDA microstructure by covalently connecting with DHI/IQ oligomers could enhance the light absorption across a broad spectrum by decreasing the energy bandgap and increasing electron delocalization (Figure 3a) [20]. Later, Bai and co-workers proposed that introducing nitrogen-containing heterocycles on PDA significantly lowers the LUMO, promoting electron delocalization in the local regions, which also resulted in the visible light absorption [21]. Moreover, the broad-spectrum light absorption capability of PDA is highly beneficial in photocatalysis. Utilizing PDA in semiconductor modification or constructing heterojunctions can expand the absorption range of semiconductors and promote charge separation. Some researches demonstrated that PDA could be used as photonic sensitizers for enhanced photocatalysis of ZnO in the range of visible light. For instance, Dong et al. fabricated a water purification membrane (PDA/ZnO-NWs/PVDF) by DA polymerization on the ZnO-NWs/PVDF surface [22]. The UV-vis-DRS was shown in Figure 3b, the introduction of PDA has significantly improved the material's absorbance to light in the range of 396−1750 nm. Similarly, by modifying PDA, the light utilization range can be extended from UV to visible light, which can also be applied to other semiconductors, such as TiO_2 and graphitized carbon nitride (g-C_3N_4) [23–25].

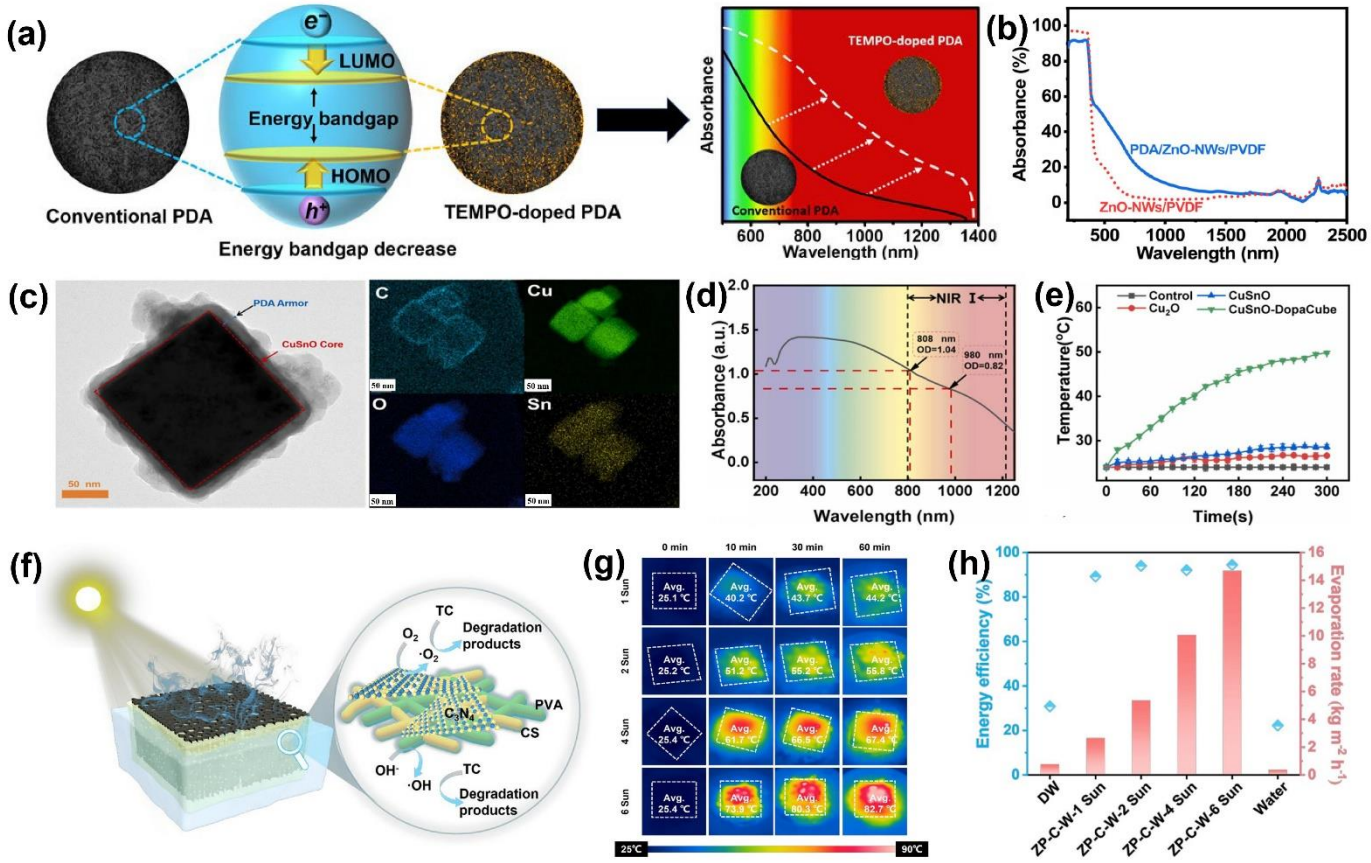

Figure 3. (**a**) The schematic illustration of the bandgap and light absorption ability of PDA and TEMPO-doped PDA [20]. (**b**) Light absorption ability of PDA/ZnO-NWs/PVDF and ZnO-NWs/PVDF [22]. (**c**) TEM image of CuSnO-DopaCube and distribution of corresponding elements. (**d**,**e**) UV-Vis absorbance spectrum and the evaluation of photothermal properties of CuSnO-DopaCube [26]. (**f**) Schematic illustration of ZIF-8@PDA/C_3N_4 coating on the wood hydrogel. (**g**) IR images of the ZP-C-W in different solar illuminations. (**h**) The corresponding evaporation rates and solar evaporation efficiencies of different photocatalysts [27].

PDA excels in photothermal conversion due to its remarkable light absorption capacity, effectively absorbing light from the visible to the near-infrared spectrum. It converts absorbed light into heat energy through non-radiative relaxation processes, where electron excitation energy is transformed into molecular vibrational energy, subsequently released as heat. The molecular structure of PDA not only facilitates efficient photothermal conversion but also enables rapid heat transfer via intermolecular interactions. Additionally, its robust thermal stability allows it to retain structural integrity at elevated temperatures, establishing PDA as a potent material for photothermal applications [28]. Gao and co-workers developed a Cu-Sn-PDA photocatalytic Fenton system [26]. As the TEM images shown in Figure 3c, the heterojunction structure fabricated by Cu_2O and SnO_2 significantly as a core, which was closely wrapped by PDA. The mapping images also confirmed the successful synthesis of the three-layered heterostructure, the element mapping showed a uniform mixture of Cu, Sn, O, and C elements, indicating that the Cu/Sn heterostructure was tightly wrapped by PDA. Firstly, the CuSnO-DopaCube's optical density (OD) values were detected through UV full spectrum (Figure 3d). The CuSnO-DopaCube (500 μg·mL^{-1}) had an OD value of 1.04 at 808 nm and 0.82 at 980 nm, indicating better photo-thermal conversion efficiency in the NIR region. In addition, the PDA coating in CuSnO-DopaCube significantly improved the photothermal performance (Figure 3e).

Based on the excellent light absorption properties across a wide spectrum of light and high photothermal conversion efficiency, PDA as a light absorption layer was well developed in solar evaporator. The solar thermal evaporation process offers a promising technology for producing thermal energy for promoting reaction dynamics and thermodynamics [29]. Lu et al. designed and fabricated a wood/ZIF-8/PDA composite and applied to the solar evaporation and water purification with the photothermal conversion efficiency of 92%. Among them, the black PDA coating on the wood surface used as light absorption layer [30]. Based on the wood/ZIF-8/PDA composite, the group members designed a wood-based hydrogel evaporator modified by C_3N_4 and PVA/chitosan hydrogel, which accelerate solar desalination and remove pollutants from wastewater (Figure 3f) [27]. As displayed in Figure 3g,h, the evaporator surface

temperature increased with the increasing solar intensity. The highest surface temperature and energy conversion efficiency under 6 kW/cm^{-2} after 60 min could reach up to 82.7 °C and 94.42%, respectively. The excellent solar evaporation performance was contributed to the solar spectra utilization of PDA.

In brief, the great light absorption and photothermal conversion properties allow PDA to improve solar energy utilization. Apart from PDA, the light absorption capacities of other common photocatalytic polymers include polyaniline (PANI) [19,31], polypyrrole (PPy) [32] and poly(3,4-ethylenedioxythiophene):poly(styrene sulfonate) (PEDOT:PSS) [33,34] are more limited than that of PDA, and it has fewer active sites [35]. For example, PANI and PPy have good light absorption ability in the UV region, but their performance in the visible region is relatively weak. Some polymers can enhance their photocatalytic properties in the form of doping or composites, but in general additional modifications are required to achieve the effect of PDA.

3.2. Surface Adhesion

The catechol and amine groups on the PDA surface make it a good substrate or template for the chelating metal ions [36]. Wang et al. synthesized PDA/CdS nanocomposite for Rhodamine B (RhB) removal from aqueous solutions [37]. First, the PDA nanoparticles were synthesized uniformly with a spherical structure (Figure 4a). Then followed by depositing CdS nanoparticles on the PDA substrate. A possible explanation may be that Cd^{2+} ions chelated with the PDA substrate, which promoted a heterogeneous nucleation of CdS nanoparticles (Figure 4b). In photocatalytic in removing RhB process, the PDA NPs in nanocomposite with the functional groups, such as −OH and $-NH_2$, exhibited the excellent absorption effect for RhB. In conclusion, it was inferred that there was a significant synergy between adsorption and degradation to efficiently remove RhB from the reactions. Additionally, PDA served as an effective shell material for constructing core-shell structures, encapsulating nanoparticles to enhance their stability. Throughout its formation, dopamine monomers polymerize at various sites to create a cross-linked network, boosting the mechanical stability and adhesive properties of the polymer film. PDA demonstrated superior interfacial activity, capable of self-assembling onto diverse material surfaces to form a uniform coating. Its molecules naturally orient at the liquid-solid interface, creating a dense film that underpins its exceptional adhesive qualities [38]. As shown in Figure 4c, the PDA coating of the core-shell structure was spontaneously formed by immersing the core structure material in an alkaline aqueous solution of dopamine [39]. The sandwich structure was a three-layer concentric heterostructure composed of two or more materials, which exhibited stronger synergistic effects comparing with traditional two-component core-shell structures [10,40–42]. Shang et al. synthesized the novel recyclable Fe_3O_4@PDA/CuS core-shell structure photocatalyst through by in situ reduction method [43]. Among them, the Fe_3O_4 was used as a magnetic core to provide recovery ability, then the PDA coated on Fe_3O_4 by self-polymerization. The PDA coating can prevent Fe_3O_4 from being oxidized, and the abundant -OH and $-NH_2$ can chelate copper ions. The Fe_3O_4@PDA/CuS exhibited excellent photocatalytic performance and cycle stability for MB degradation.

Therefore, the rich active groups on the surface of PDA enable it to form strong adhesion with a variety of material surfaces, which can be used as a bonding layer to immobilize the photocatalyst on various substrates and increase the stability and service life of the photocatalyst. Compared with PDA, PANI, PPy and PEDOT: PSS exhibited weak adhesion, especially in wet environment, but it can still be enhanced through chemical modification or by introducing a hydrophilic polymer adhesive layer to improve its surface adhesion properties [44,45].

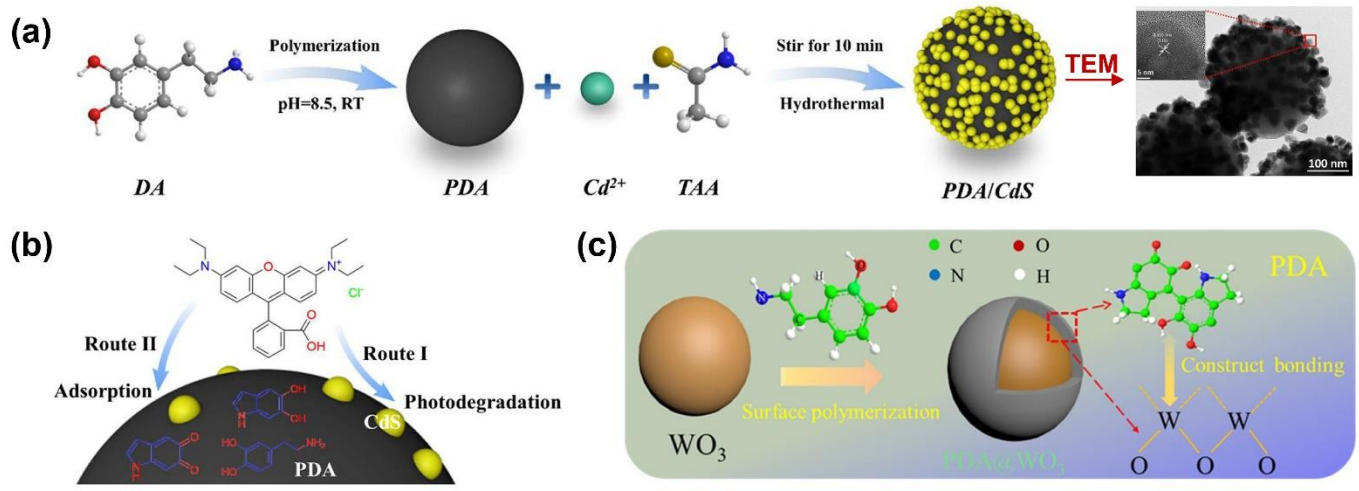

Figure 4. (**a**) The preparation process of PDA NPs/CdS nanocomposite and (**b**) the RhB degradation process [37]. (**c**) Preparation process of the PDA@WO_3 nanocomposite [39].

3.3. Film Forming Properties

As inspired by mussels' foot proteins mfp, a strong attachment to almost all substrate types have made PDA one of the most popular coating methods. So far, PDA coatings have been used as mechanical strength coatings combined with porous materials, such as hydrogel [46], foam [47], sponges [48,49] and cotton fabrics [50,51]. On the one hand, this ability to uniformly coat different materials ensures that the light absorption layer is stable and durable, maintaining its efficiency over time. On the other hand, the modification of PDA on the substrates will further enable strong binding of photocatalysts on the substrate, benefiting the stability and recyclability of the photocatalyst. Li et al. reported a novel recyclable cotton fabric/PDA/BiOBr (CFPB) photocatalyst prepared by immobilizing the BiOBr component on PDA modified cotton fabric, which was used for RhB removal and Cr(VI) reduction in visible light irradiation (Figure 5a) [52]. Gong et al. synthesized a novel coated photocatalyst based on the polydopamine modified melamine sponge and then adhering Ag-AgCl/WO_3/g-C_3N_4 (AWC) nanoparticles (Figure 5b) [53]. The AWC/PDA/MS removed 99.9% of trimethoprim (TMP) under visible light in 90 min. The recyclable photocatalyst based on a PDA modified flexible substrate provides a green alternative to powdered photocatalysts with low recyclability. PDA have been used as a component in a number of different filtration membranes, such as PAN and PVDF [54,55]. For instance, Wang et al. designed a 3D layered photocatalytic fiber membrane PAN@PDA/Tb-g-C_3N_4/$ZnIn_2S_4$ (PPTZ), by electrospinning and coating process (Figure 5c). First, the PAN@TCN fiber films (layer 1) were obtained via electrostatic spinning. Then PDA was deposited on the PT membrane via in situ self-polymerization, which was acted as an intermediate linker. Lastly, the $ZnIn_2S_4$ was uniformly deposited on the membrane surface, then the three-dimensional layered membrane was labelled as PPTZ. Such a fibrous film had excellent photocatalytic degradation efficiency of antibiotics.

In conclusion, PDA forms stable coatings on various substrates with its simple film formation process, excellent adhesion, and surface uniformity, while the film formation of other polymers is more complex, often requiring specific control of conditions, and has advantages in electrical conductivity and mechanical properties [45]. Therefore, PDA is relatively more advantageous in the field of photocatalysis.

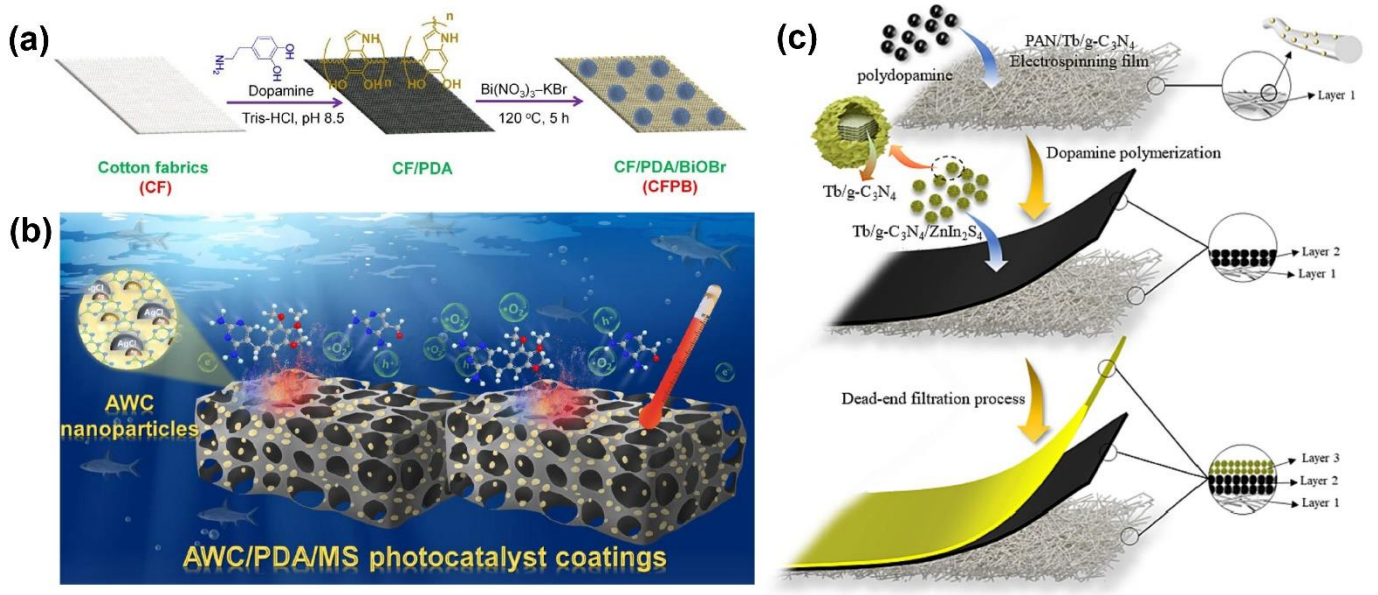

Figure 5. (**a**) The preparation process of photocatalyst fabrics CFPB [52]. (**b**) The schematic of photocatalytic degradation of TMP with AWC/PDA/MS photocatalyst coatings [53]. (**c**) The synthetic pathway of the PPTZ film [56].

3.4. Conductivity

Polydopamine (PDA), as an organic polymer, is not a conductive material in the traditional sense, but it has certain conductivity. This is mainly due to the aromatic ring structure contained in the PDA molecule forming a certain conjugated system. These conjugated systems allow π electrons to move easily between molecules, thereby giving PDA a certain conductivity [57]. Second, PDA exhibits significant π–π interactions due to its unique molecular structure, which contains aromatic rings. These π–π interactions contribute to several important properties and applications of PDA [38]. For example, the π–π interactions enable PDA to strongly adsorb onto surfaces containing aromatic rings or π-conjugated systems [58]. Additionally, the strong interactions facilitate electron transfer processes, contributing to the overall catalytic performance. Graphitized carbon nitride (g-C_3N_4) is a 2D metal-free π-conjugated polymer semiconductor photocatalyst with a wide range of applications in photocatalysis [59]. The conjugated π structure shared between PDA and g-C_3N_4 allows π-π* electrons delocalization, which synergistically enhanced carrier transport. Therefore, modifying g-C_3N_4 with PDA can enhance the activity [15,60]. Furthermore, the bridge-like channel structure formed by the PDA could induce charge transfer through the additional electron transfer channel (PDA), forming the direct Z-scheme charge transfer mechanism [61–63].

Wu and colleagues constructed a Z-Scheme Bi@$Bi_2O_2CO_3$/PDA/g-C_3N_4 (BPCN) heterojunction [64]. As illustrated in Figure 6a, during the polymerization process, PDA adhered to g-C_3N_4 through strong covalent and non-covalent interactions, as well as π-π* stacking, and provided additional pathways for electron transfer. Thereby enhancing photocatalytic performance through synergistic effects on light absorption and charge carrier separation. The possible photocatalytic mechanism of BPCN heterojunction was proposed in Figure 6b. In the internal electric field formed between $Bi_2O_2CO_3$ and g-C_3N_4, electrons rapidly flow from the conduction band of $Bi_2O_2CO_3$ to the valence band of g-C_3N_4. They then recombine with the holes on g-C_3N_4 via PDA acting as an electronic bridge. The conjugated π-π* structure between g-C_3N_4 and PDA facilitated electron delocalization and carrier transfer, balancing the Fermi levels between the semiconductors. Similarly, PDA bridge acted as cross-link of the active phase on carbon nitrates (g-C_3N_4) to ZnAl layered double hydroxide nanosheets to construct VL-driven Z-type heterojunction catalysts [61].

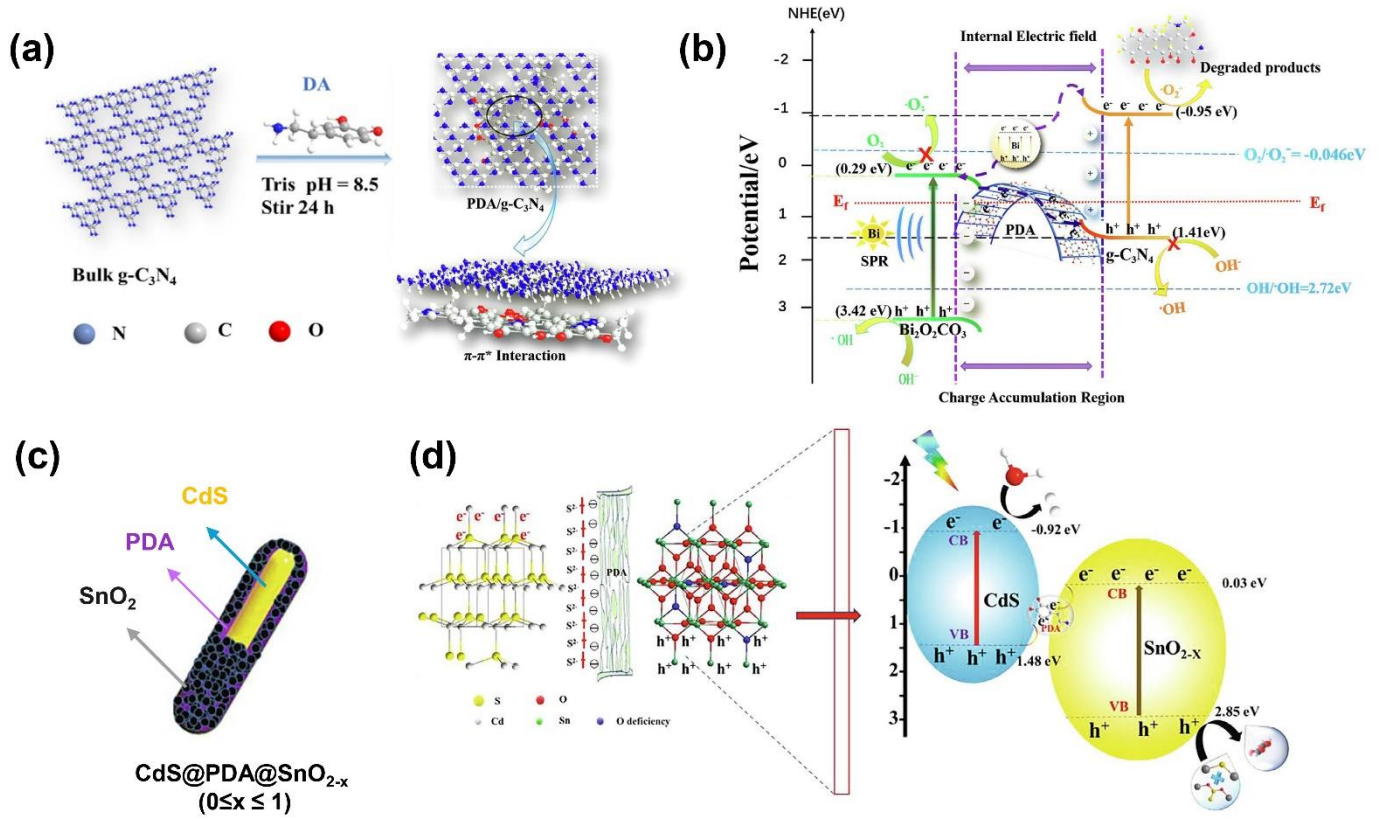

Figure 6. (**a**) The preparation process of PDA/g-C_3N_4 and (**b**) the possible mechanism of charge transfer of BPCN under visible light irradiation [64]. (**c**) The sandwich structure of CdS@PDA@SnO_{2-x} and (**d**) the photoelectron transfer of CdS@PDA@SnO_{2-x} [65].

In sandwich structure composites, PDA can not only prevent photocorrosion of the nuclear structure, but also served as photosensitizer and electron transfer mediator in the heterojunction [51,66]. Liu and co-workers constructed a CdS@PDA@SnO_{2-x} heterojunction with sandwich structure (Figure 6c) [65]. In this structure, PDA molecules wraped around the surface of CdS, protecting the core from photocorrosion. Simultaneously, the catechol structure of PDA can anchor Cd^{2+} and Sn^{4+} ions at specific positions, leading to quick electron transfer, as illustrated in Figure 6d. The as-prepared photocatalyst exhibited an excellent photocatalytic hydrogen (H_2) production activity. Qin et al. synthesized a CdS@PDA/NiS ternary composite for H_2 production [40]. The strong Cd–O chemical bond between CdS and PDA served as high-speed electron transmission channels, while the Schottky junction accelerated the spatial separation of carriers and improved the photocatalytic hydrogen production performance. After four experiment cycles, the obtained CdS@PDA/NiS maintained good photocatalytic activity and structural integrity.

PDA with conjugated systems has excellent electron transport capability, which can reduce the recombination of electron-hole pairs during photocatalysis. Apart from PDA, other common photocatalytic polymers (such as PANI and PPy) also exhibited excellent electrical conductivity and stability [67,68]. This property allows them to conduct electrons efficiently and promote the separation of electrons from holes in the photocatalytic reaction, thereby improving the photocatalytic efficiency.

4. Regulation Strategies of PDA in the Field of Photocatalysis (Mainly Composite Materials with Various Semiconductors)

4.1. Directly Construct Composite Materials with PDA and Other Semiconductors

PDA is a kind of polymer material with unique chemical structure and functional groups, which has received wide attention for its potential application in photocatalysis. At present, the photocatalytic performance of PDA can be improved by metal ion doping and constructing composites with other semiconductors (or plasma metal monomers) or surface modification [69–75]. In the construction of photocatalytic composites, PDAs are often mainly used to form heterojunctions with other semiconductor materials (the main types include: direct to electron conduction type, type II, Z-scheme and S-scheme) to improve the photocatalytic performance. Commonly, g-C_3N_4 [58,76–79], metal oxides (TiO_2, ZnO, Cu_2O, CeO_2, etc.) [80–86], Bi-based materials (BiOCl, $Bi_{2.15}WO_6$ etc.) [87–90], metal sulfides (CdS, ZnS,

ZnCdS, $ZnIn_2S_4$, etc.) [91–94], MOFs [95,96], metal alloys [97–99] and carbon dots [100] are used to construct composites directly with PDA. By compositing PDA with these semiconductor materials, it is possible to enhance the photocatalytic efficiency and at the same time extend its application in the visible light range, thus realizing more efficient photocatalytic reactions. Jing and co-workers designed a 1D CdS/PDA heteronanotubes (HNTs) photocatalyst for antibiotic degradation (Figure 7a) [93]. Under the light excitation, the oxygen was reduced into $\bullet O_2^-$ by photoexcited electrons or continuously converted into •OH to attack the antibiotics. On the other hand, h^+ in the valence band can also attack the antibiotics directly and trigger continuous degradation. A Cu_2O@PDA nanospheres composite was designed by Zhou and co-workers for methylene orange (MO) dye degradation (Figure 7b) [84]. Cu_2O and PDA exhibit energy level alignment suitable for the construction of a type II heterojunction. Based on this mechanism, the electrons accumulated on the PDA surface and reacted with water and oxygen to produce ROS (including •OH and $\bullet O_2^-$), while the h^+ focused on the valence band (VB) of Cu_2O. Under the oxidation of ROS and h^+, MO was degraded into CO_2, H_2O, etc. Shi et al. constructed a polydopamine-coated tungsten oxide (PDA@WO_3) nanomaterial with special yolk-shell structures (Figure 7c) [39]. The WO_3 and PDA can form a Z-Scheme transport mechanism in photocatalytic reactions and lead to a lifetime extension of the carriers. Specifically, under light illumination, the PDA in PDA@WO_3 induces a π–π transition, where excited-state electrons are transferred from the highest occupied molecular orbital (HOMO) to the lowest unoccupied molecular orbital (LUMO) of PDA, leaving behind a large number of holes (h^+). The electrons generated from WO_3 are transferred to the HOMO orbital of PDA through interfacial transport under the effect of built-in electric field, and these electrons are combined with holes in HOMO. The electrons in the LUMO orbital of PDA could reduce O_2 to $\bullet O_2^-$, which react directly with the MB. Zhang et al. synthesized a novel S-scheme heterojunction photocatalyst comprised of ultrathin g-C_3N_4 (U-CN) and PDA [12] (Figure 7d). Under light irradiation, electrons in U-CN were excited from their VB to conduction band (CB) and eventually recombined with the holes in the HOMO of PDA driven by the built-in electric field, manifesting the S-scheme mechanism.

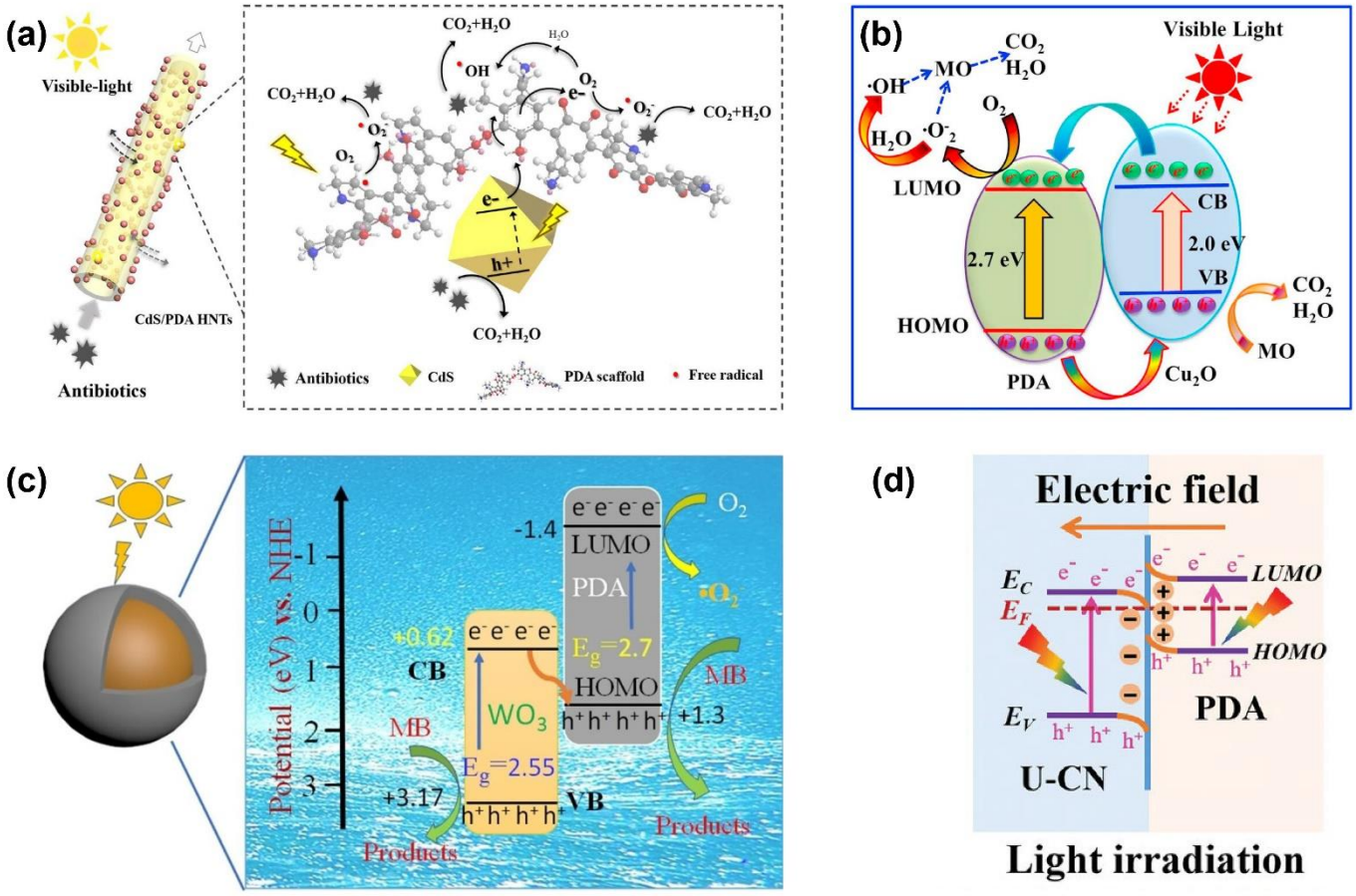

Figure 7. (**a**) Schematic diagram of the reaction mechanism during the catalytic decomposition of antibiotics by CdS/PDA [93]. (**b**) Schematic diagram of the possible photodegradation mechanism of Cu_2O@PDA via visible light irradiation [84]. (**c**) Schematic diagram of the photodegradation mechanism of MB on PDA@WO_3 sample [39]. (**d**) Schematic diagram of the S-type photocatalytic mechanism of C_3N_4/PDA [12].

4.2. Composite Materials Constructed with PDA as an Electronic Bridge Structure

PDA as an electronic bridge plays multiple advantages in photocatalytic composites, including improving the separation efficiency of photogenerated electrons and holes and forming multifunctional composite structures with a variety of semiconductors to realize diversified photocatalytic reactions, which shows its potential for application in building highly efficient and stable photocatalytic materials [101–104]. Zhang et al. developed a ZnO@PDA-Au photocatalytic system for organic pollutant removal (Figure 8a) [105]. When Au contacts ZnO, a Schottky barrier forms due to work function differences, and ZnO under UV-visible light excitation generates electron-hole pairs. Electrons transfer from ZnO to Au and PDA, reducing dissolved oxygen to create $\bullet O_2^-$, while holes oxidize water to form •OH. These radicals contribute to organic molecule degradation. The PDA and local surface plasmon resonance (LSPR) effect of Au enhanced visible light absorption. The Schottky barrier served as an electron trap utilizing charge separation efficiency and significantly and boosting the catalytic performance of ZnO@PDA-Au. Figure 8b illustrates that AgNPs/PDA/g-C_3N_4 enhances the charge step transfer route via the built-in electric field, with PDA capturing molecular oxygen to generate free radicals and improve pollutant adsorption. The LSPR effect of AgNPs was triggered at a wavelength of 390–420 nm, producing hot electrons and reducing the electron-hole recombination rate, which increased the generation rate of charge carriers. This synergy between PDA and AgNPs significantly boosted the photocatalytic MB degradation activity of g-C_3N_4 [106]. Figure 8c illustrated the photocatalytic hydrogen production mechanism developed by Meng et al. using a g-C_3N_4 nanotube@PDA/NiCo-LDH composite. Under visible light, g-C_3N_4 and NiCo-LDH generated electron-hole pairs, with PDA acting as a photosensitizer and interface medium to boost light absorption and facilitate charge transport. The electrons from g-C_3N_4 were drawn to the higher energy levels of NiCo-LDH, while the holes migrated to g-C_3N_4. Pt nanoparticles catalyzed the reaction of electrons on NiCo-LDH with H+ ions in water to produce hydrogen, whereas holes on g-C_3N_4 were quenched by TEOA. The combined action of the type II heterojunction and PDA significantly enhances carrier separation and transport, greatly improving the efficiency of hydrogen production [107]. Yang et al. developed a type II heterostructure by combining carbon nitride nanosheets (CNNS) with CdS, which under light exposure, facilitated the production of photogenerated electron-hole pairs (Figure 8d) [15]. Electrons were transferred from the CB of CNNS to the CB of CdS, while holes migrated from the VB of CdS to the VB of CNNS. The electrons in CdS reacted with dissolved oxygen to produce superoxide radicals ($\bullet O_2^-$), and the holes in CNNS directly participated in the degradation of RhB. The inclusion of polydopamine (PDA) in this setup enhanced charge migration, minimized electron-hole recombination, and thus significantly bolstered the photocatalytic efficiency. A novel g-C_3N_4@PDA/BiOBr Z-scheme photocatalytic system was constructed by Guo et al. (Figure 8e) [62]. Here, electrons move from the CB of BiOBr to the VB of g-C_3N_4 through PDA, leading to effective charge separation. This movement resulted in a higher concentration of electrons in the CB of g-C_3N_4 and holes in the VB of BiOBr. The holes in BiOBr's VB are potent enough to directly oxidize sulfamethoxazole (SMX), while the accumulated electrons in g-C_3N_4's CB reduce O_2 to form superoxide radicals ($\bullet O_2^-$). Concurrently, the VB holes in BiOBr can also oxidize H_2O/OH^- to generate hydroxyl radicals (•OH). These radicals collaborate to decompose SMX into CO_2 and H_2O. PDA serves a crucial role as an electron mediator, enhancing carrier separation and thereby boosting the photocatalytic redox capabilities of the composite material.

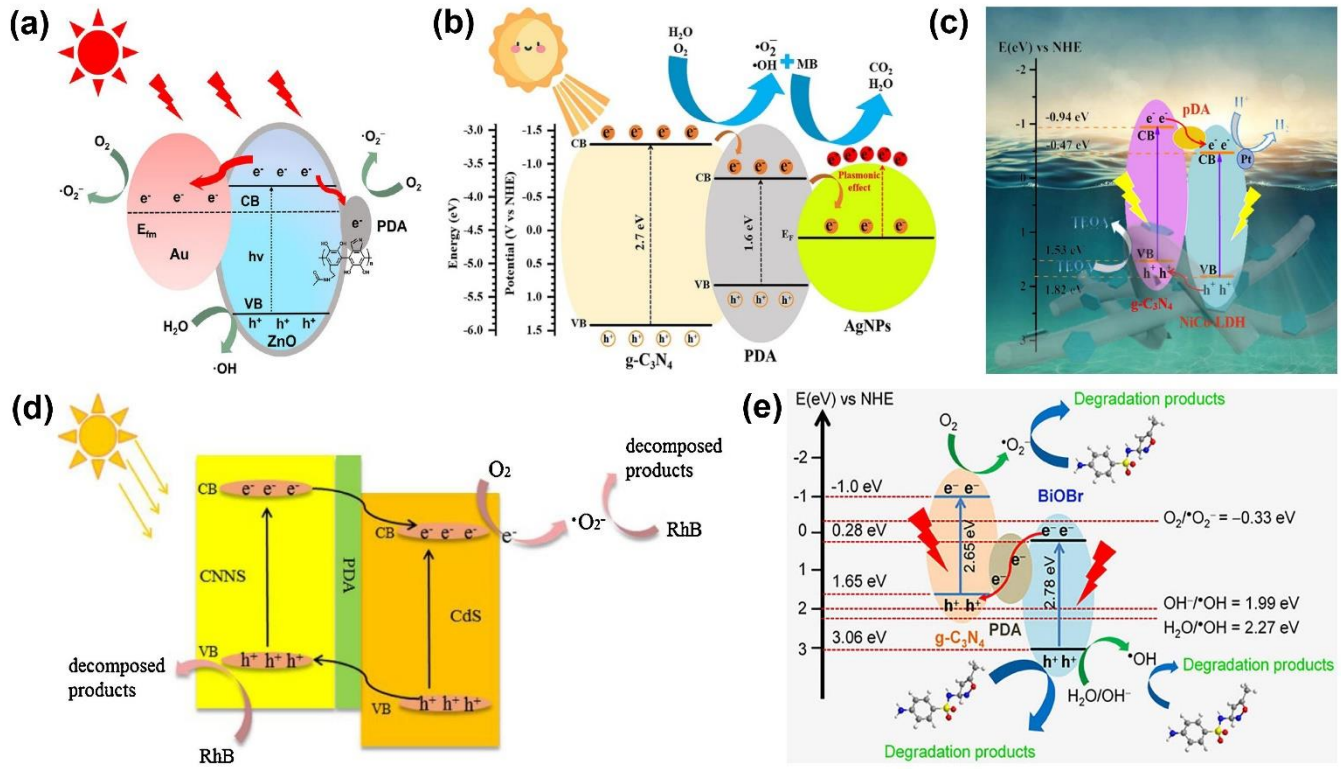

Figure 8. (**a**) Mechanism diagram of ZnO@PDA-Au under UV-visible light irradiation [105]. (**b**) Schematic diagram of charge migration of AgNPs/PDA/g-C_3N_4 [106]. (**c**) Possible mechanism of photocatalytic hydrogen production by g-C_3N_4@pDA/NiCo-LDH [107]. (**d**) Possible mechanism of photocatalytic removal of RhB by CNNS/PDA/CdS [15]. (**e**) Possible mechanism of photodegradation of SMX by Z-scheme heterojunction g-C_3N_4@PDA/BiOBr under visible light irradiation [62].

4.3. Comprehensive Photocatalytic System Constructed by Combining PDA, Semiconductor and Membrane Materials (Other Carrier Materials)

The photocatalytic system fabricated by combining PDA, semiconductor and membrane materials utilizes the excellent film-forming and surface modification capabilities of PDA to form a uniform protective layer on the surface of the semiconductor material, which enhances stability and durability [108–114]. The hydrophilicity and anti-pollution properties of the PDA-modified membranes enhance the efficiency of wastewater treatment and simplify the cleaning and regeneration process. The biocompatibility and environmentally friendly synthesis process of PDA support the construction of sustainable photosynthetic systems. Membrane materials provide physical protection for the photocatalysts and prolong the service life, while PDA enhances the surface activity and reaction sites to accelerate the photocatalytic reaction rate. The composite system of PDA, semiconductor, and membrane materials (PES, PVDF, cellulose membrane, PVA, cellulose acetate membrane, PET, poly (arylene ether nitrile) (PEN), polyacrylonitrile (PAN), polytetrafluoroethylene (PTFE), etc.) is simple to prepare, easy to produce on a large scale, and multifunctional. Overall, the photocatalytic system constructed by PDA, semiconductor and membrane materials significantly improves the photocatalytic efficiency by improving the photocatalytic activity, stability, enhanced the surface properties and multifunctionality, and shown a wide range of application potential [115–121]. Shi et al. developed a poly (vinylidene fluoride) (PVDF) composite membrane enhanced with polydopamine and titanium dioxide nanoparticles, designed for efficient and eco-friendly treatment of organic wastewater (Figure 9a) [55]. After UV irradiation for 60 min, this membrane exhibited a water flux three times higher than that of the standard PVDF membrane. It showed remarkable pollutant retention, removing approximately 99.0% of Congo red and Coomassie Brilliant Blue G250. Post-treatment, the water flux of the membrane recovered over 87.2%. Additionally, the composite membrane demonstrated excellent retention and antifouling capabilities in oil-water emulsion filtration, underscoring its versatility in various wastewater treatment and separation applications. Zheng et al. developed a novel photocatalytic nanofiltration (NF) membrane by applying interfacial polymerization on PVDF membranes to introduce a polyamide layer and incorporating polydopamine with $BaTiO_3/Ti_3C_2T_x$ nanoparticles (Figure 9b) [110]. This combination achieved both physical separation and photocatalytic degradation functionalities. The membrane demonstrated high water permeability (34.0 $L \cdot m^{-2} \cdot h^{-1} \cdot bar^{-1}$) and excellent Na_2SO_4 retention (94.7%). Under irradiation from a 300 W Xe lamp for 180 min, it showed substantial photocatalytic

degradation efficiencies for various azo dyes: 95.3% for methyl orange (MO), 92.7% for alizarin yellow GG, and 83.5% for methyl red. This research introduces an innovative approach for creating bifunctional photocatalytic nanofiltration membranes with effective degradation capabilities. In addition to the membrane materials mentioned above, more types of carrier materials (polyurethane sponge, cellulose fibers, nickel foam, hydrogel, woven cotton fabric, wood, melamine foam, filter paper, etc.) can replace membrane materials [122–128], further promoting the practical application value of PDA-based photocatalytic materials.

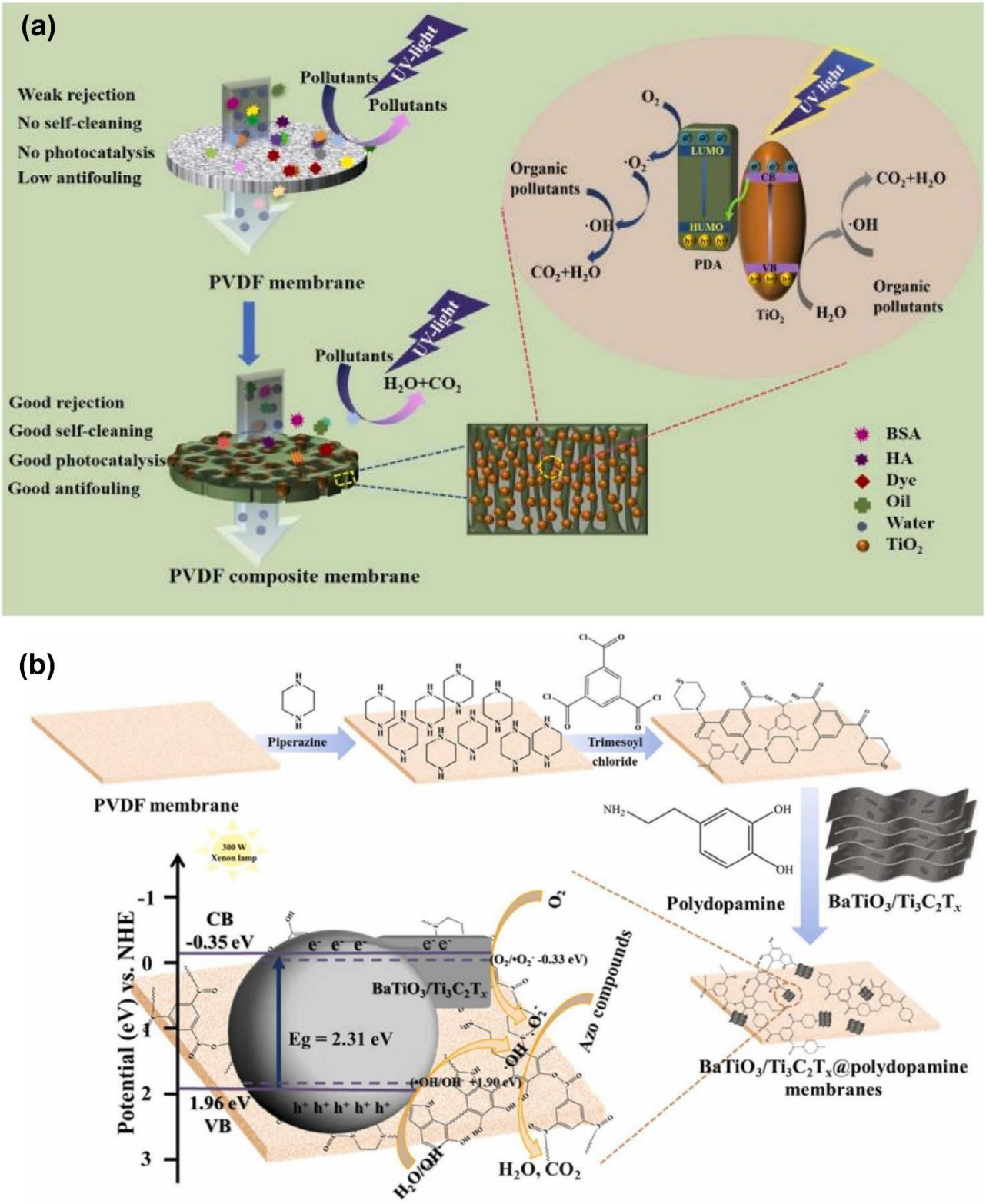

Figure 9. (**a**) PVDF/PDA-TiO_2 composite membrane for filtration of pollutants photodegradation [55]. (**b**) Schematic diagram of the $BaTiO_3/Ti_3C_2Tx$@PDA membrane manufacturing process and the photodegradation mechanism of the $BaTiO_3/Ti_3C_2Tx$@PDA membrane [110].

5. Application of PDA in the Field of Photocatalysis

As a typical organic polymer material, PDA itself has very poor photocatalytic activity. Nevertheless, PDA-based photocatalysts have attracted much attentions owing to their excellent properties, such as light harvesting abilities, interfacial properties and electron transfer capabilities. Hence, PDA can synergize with semiconductor photocatalysts to enhance photocatalytic performance in various application fields. In this part, we give a brief overview of their application areas in water purification, water splitting, carbon dioxide reduction and other photocatalytic reactions.

5.1. Water Purification

In recent years, the shortage of water resources has become increasingly serious, and water pollution has exacerbated the shortage problem. The main pollutants include organic pollutants, heavy metal ions, microbes and bacteria. Photocatalytic technology has become an important, economical and effective method to solve environmental pollution problems.

5.1.1. Organic Pollutants Degradation

PDA, with rich functional groups and unique structure, exhibits significant absorptivity for organic pollutants, making it a valuable material in environmental remediation. For example, the aromatic rings of PDA molecular structure can engage in π-π interactions with the aromatic rings of organic pollutants molecules, improving adsorption capacity. This interaction is particularly effective for adsorbing organic pollutants with aromatic ring structures, such as azo dyes and aromatic compounds [129–131]. Besides, electrostatic attraction or repulsion between the surface charge of the catalyst and the pollutant molecules affects adsorption performance. For example, a positively charged catalyst surface is more likely to adsorb negatively charged pollutant molecules. The surface charges of PDA are controllable by adjusting the pH medium [63]. Recently, an Ag/PDA@Ag_2S smart pH-heterojunction photocatalyst with multi interface band structure modulation was designed and proposed through a simple and rapid in situ polymerization method (Figure 10a) [132]. The photocatalytic process was carried out with Ag/PDA@Ag_2S for the four cationic and anionic dyes and, at the same time, the PDA-free photocatalyst was used as a reference. As shown in Figure 10b,c, it was observed that the Ag/PDA@Ag_2S s could successfully degrade cationic dyes with remarkably higher efficiency than anionic dyes. Specifically**,** methylene blue (MB) was degraded by 80% after 10 min, while MO was degraded by about 4.0%, which was proven visually by the color change as well. In addition to improving charge transport and separation, the ultra-thin layer shell introduced by PDA increases the photostability of Ag_2S/Ag photocatalysts. The PDA has the unique capability to switch on and off Ag/Ag_2S hybrid photocatalysts depending on the pH or ionic strength of the reaction medium, resulting in selective photodegradation of organic dyes. Recently, Daniel et al. explored the influence of PDA coating on the electronic effects of Au particles and tested the photocatalytic performance with Rhodamine 6G (Rh6G) [133]. As shown in Figure 10d, the Au/PDA hybrid nanoplatform was synthesized by an AuNR core followed by the further self-polymerization of PDA. The thickness of the PDA was influenced by the concentration of dopamine hydrochloride. Figure 10e illustrated the RhG6 degradation efficiency under different photocatalysts, indicating the higher photocatalytic efficiency of Au/PDA composites than that of Au and PDA particles alone and increased with the with the PDA thickness, where the degradation of AuNRs/PDA3 could reach up to 50% in 60 min. It was analyzed that the Au/PDA nanoparticles could generate reactive oxygen species (ROS) by the absorbed heat both in the visible and NIR regime (Figure 10f). When combined with the Au, the heat pump into the PDA, which could strengthen and drive the production of ROS of •OH and $\bullet O_2^-$. In addition, due to the photothermal effect and the release of ROS, the PDA modified plasmonic metal photocatalyst has excellent antibacterial properties in waste water treatment.

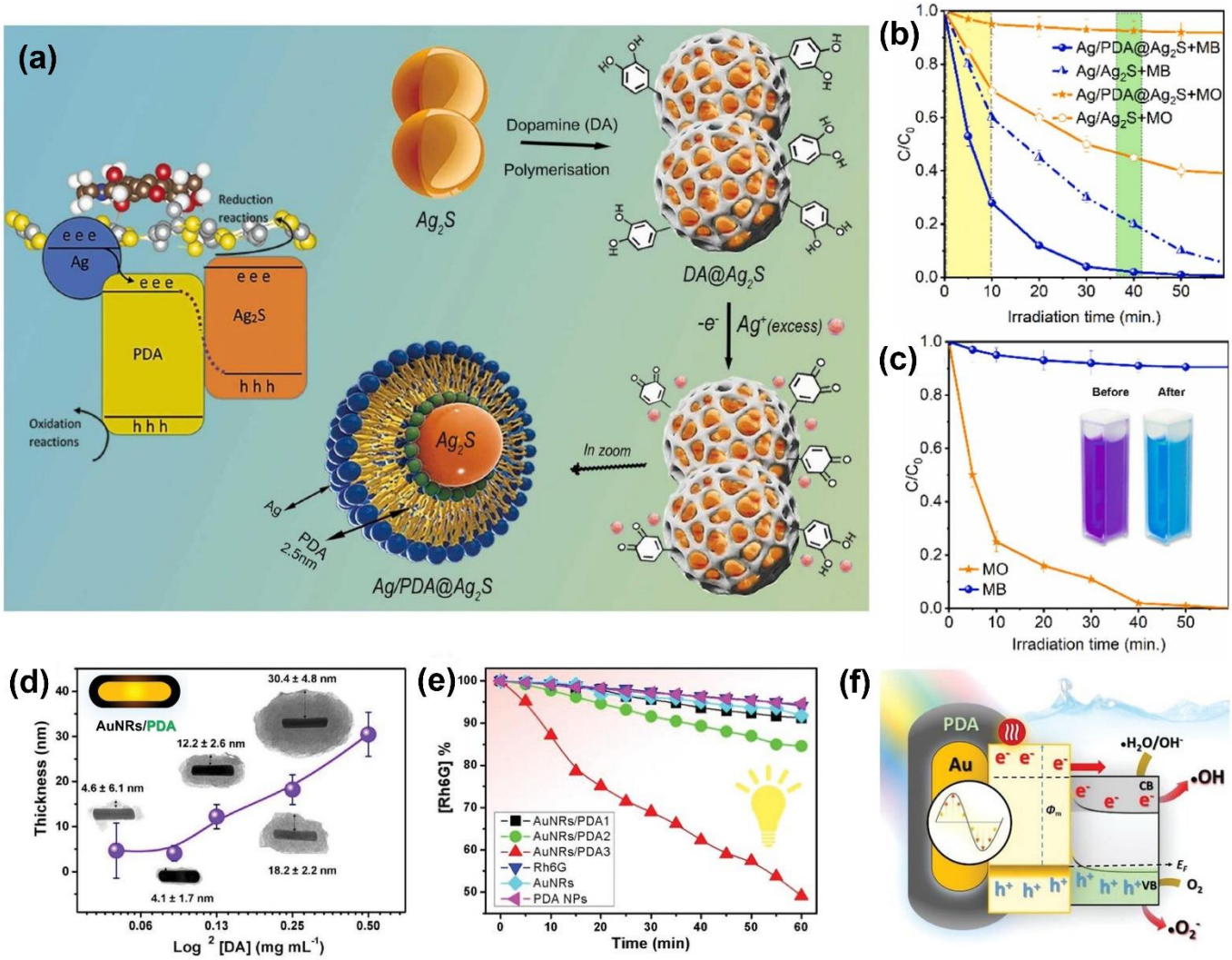

Figure 10. (**a**) The Ag/PDA@Ag_2S smart heterojunction photocatalyst for dyes photocatalytic degradation. (**b**) Photocatalytic degradation efficiency of MB and MO at pH = 10. (**c**) Plots of photodegradation of MB and MO mixture against Ag/PDA@Ag_2S smart photocatalyst at pH = 2 [132]. (**d**) PDA shell thickness (with SD) versus $\log^2$[DA]. (**e**) Percentage of Rh6G concentration depleted versus time of different photocatalysis. (**f**) Band model of the general production of ROS during VIS irradiation [133].

5.1.2. Heavy Metal Ion Reduction (Cr(VI))

PDA has a large number of hydroxyl and amino functional groups, which can chelate with metal ions, effectively adsorbing and removing heavy metal ions from water, thereby improving water treatment efficiency. The reduction of Cr(VI) ions typically involves converting to Cr(III), which is less toxic and more stable in the environment [134]. For example, Lu et al. synthesized PDA/AgNPs through the self-polymerization of PDA and the *in-situ* reduction of Ag^+ to AgNPs via PDA [135]. The reaction process of Cr(VI) removal was shown in Figure 11a, the large amino groups of PDA adsorbed Cr(VI) into the surface of photocatalyst, then improving the degradation efficiency under illumination. As demonstrated in Figure 11b, the Cr(VI) removal under dark conditions and Cr(VI) concentration after illumination indicated that PDA absorption was also beneficial to Cr(VI) removal. For the existence of plentiful amino and catechol groups, the homogeneous composites combined the PDA and semiconductors through coordination and DA self-polymerization. Additionally, PDA can absorb a broad range of wavelengths, increasing light capture capabilities, thereby enhancing the activity of photocatalysts under visible light. Li and colleagues reported a part of the TiO_2-like structure Ti-PDA NPs composite for Cr(VI) reduction (Figure 11c) [69]. As shown in Figure 11d, the photoreduction rate of Cr(VI) by Ti-PDA 3 was near 99% in 30 min, which was contributed to the sensitization effect of PDA, which kept at 95.02% after three cycles. Li and co-workers reported a 0D/1D heterostructure of PDA modified hexagonal carbon nitride tubes (HCN) for the photocatalytic Cr(VI) reduction [77]. 0D PDA nanoparticles were widely distributed inside and outside the open channels of 1D HCN to promote the sufficiently photoreduction of Cr(VI) on dual surfaces, and can achieve nearly 100% reduction of Cr(VI) after 75 min. This highly efficient 0D/1D heterostructure may serve

as a guide for photocatalysts of other conjugated polymers, thereby enhancing their potential for environmental remediation and energy applications.

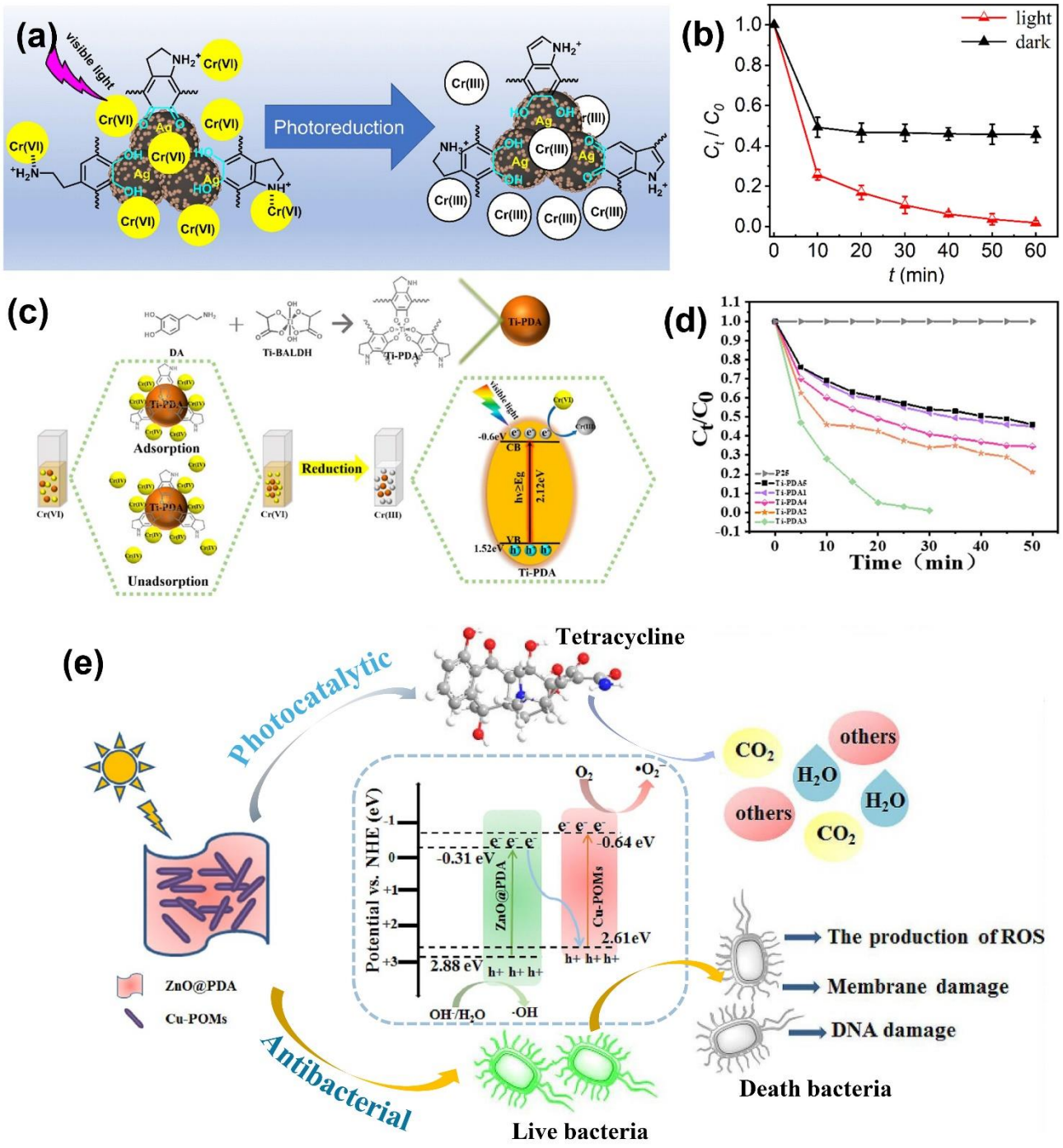

Figure 11. (**a**) The photocatalytic process of Cr(VI) through PDA/AgNPs composites. (**b**) Removal effiency of Cr(VI) under illumination or dark [135]. (**c**) Synthesis of Ti-PDA NPs and the process of Cr(VI) absorption and photoreduction. (**d**) The photoreduction curves of Cr(VI) by different photocatalyst [69]. (**e**) The possible mechanistic for tetracycline (TC) degradation and antibacterial by ZnO@PDA/Cu-POMs [136].

5.1.3. Sterilization

As be mentioned before, PDA exhibited high antibacterial efficiency under near infrared irradiation owing to the photothermal effect and photodynamic-induced ROS [42,137]. Recently, the excellent physiochemical properties and effectiveness against pathogenic microorganisms of metallic oxides have enabled them to be used for preparing photocatalyst composites for environmental remediation [138–140]. Cui and co-workers synthesized a ZnO@PDA/Cu-POMs, with high-efficiency photocatalytic degradation of TC and extraordinary antibacterial activities [136]. As shown in

Figure 11e, the ZnO@PDA/Cu-POMs heterostructure conformed to the Z-type charge transfer mechanism. Then under the attack of the reactive species, 90.75% of TC was effectively degraded. Additionally, the ZnO@PDA/Cu-POMs nanocomposite exhibited excellent antibacterial activity against 4 kinds of Gram-positive/negative bacteria, and the antibacterial rates were higher than 99% for all bacterial strains. The possible mechanistic of antibacterial action was that the ROS of ZnO@PDA/Cu-POMs could cause damage to the membrane and DNA of bacteria, then collectively induced bacterial cell death.

PDA is rich in functional groups such as hydroxyl, amine, and catechol groups, which can interact with various photocatalysts like TiO_2, ZnO, and g-C_3N_4 to form composite materials. In water purification, PDA synergistically works with photocatalysts to significantly enhance the degradation efficiency of organic pollutants such as MO and MB. The presence of PDA facilitates the generation of ROS (e.g., •OH, $•O_2^-$), which rapidly oxidize and decompose contaminants in water. PDA not only degrades organic pollutants but also chelate with metal ions, effectively adsorbing and removing heavy metal ions from water, thereby im-proving water treatment efficiency. Furthermore, PDA exhibits outstanding antibacterial properties, effectively inhibiting the growth of pathogenic microorganisms in water, thus achieving multifunctional water purification. In short, under synergy with the semiconductor photocatalyst (such as metal sulfide or metal oxide), PDA shows excellent photocatalytic effects in the fields of water purification, including organic pollutants degradation, Cr(VI) reduction and sterilization.

5.2. Water Splitting

Hydrogen, as an efficient and pollution-free energy source, can be widely used in industry, transportation, and energy storage. By producing hydrogen through photocatalytic water splitting, we can harness the inexhaustible resource of solar energy, reduce dependence on fossil fuels, decrease greenhouse gas emissions, and help address global climate change and energy crises [141–143].

As one of the most widely used water splitting materials, g-C_3N_4 has attracted considerable attention for its adjustable bandgaps and excellent physiochemical properties. In addition, the hollow g-C_3N_4 nanospheres (HCNS) stand out in the research on various novel structures of g-C_3N_4, owing to their unique hollow structure and abundant active sites. Wang et al. reported a strategy comprising the g-C_3N_4 and PDA to a hollow flower-like nanosphere (g-C_3N_4@PDA), where monodisperse polystyrene microsphere using as template [144]. The photocatalyst construction process was shown in Figure 12a. the PDA@PS nanospheres was formed via DA self-polymerizes. Specifically, the g-C_3N_4 nanosheets were then introduced onto the outer surface of the PDA@PS nanospheres via interfacial self-assembly, then removing the PS template by in $CHCl_3$. A series of photocatalysts were used to evaluate the H_2 production rates (HER) as shown in Figure 12b. A significant improvement in the HER was observed after exposure to visible light irradiated with g-C_3N_4@PDA nanospheres, which was contributed by the conjugated system and the hollow nanostructure. In addition, the HER matched well with its light absorption curve (Figure 12c). When the incident light wavelength was extended to 700 nm, the g-C_3N_4@PDA still showed good photocatalytic activity (HER = 5 μmol h^{-1}). The mechanism of optical activity was illustrated in the Figure 12d,e, based on the synergistic effect, PDA continuously supplied electrons to the CB of g-C_3N_4 while accepting holes from g-C_3N_4, thus reducing electron-hole recombination. Additionally, the hollow nanospheres with multifaceted open surface areas can facilitate surface-dependent reactions by effectively shuttling electrons and chemicals. These factors collaboratively enhance the photocatalytic performance of the nanomaterials. Similar, Yang et al. fabricated a PDA/defective ultrathin mesoporous g-C_3N_4 (PDA/DCN) Z-scheme organic for the H_2 evolution and organic degradation (Figure 12f) [145]. It was demonstrated that N-vacancy and π-π interactions provide strong connection and Z-scheme fast charge transfer.

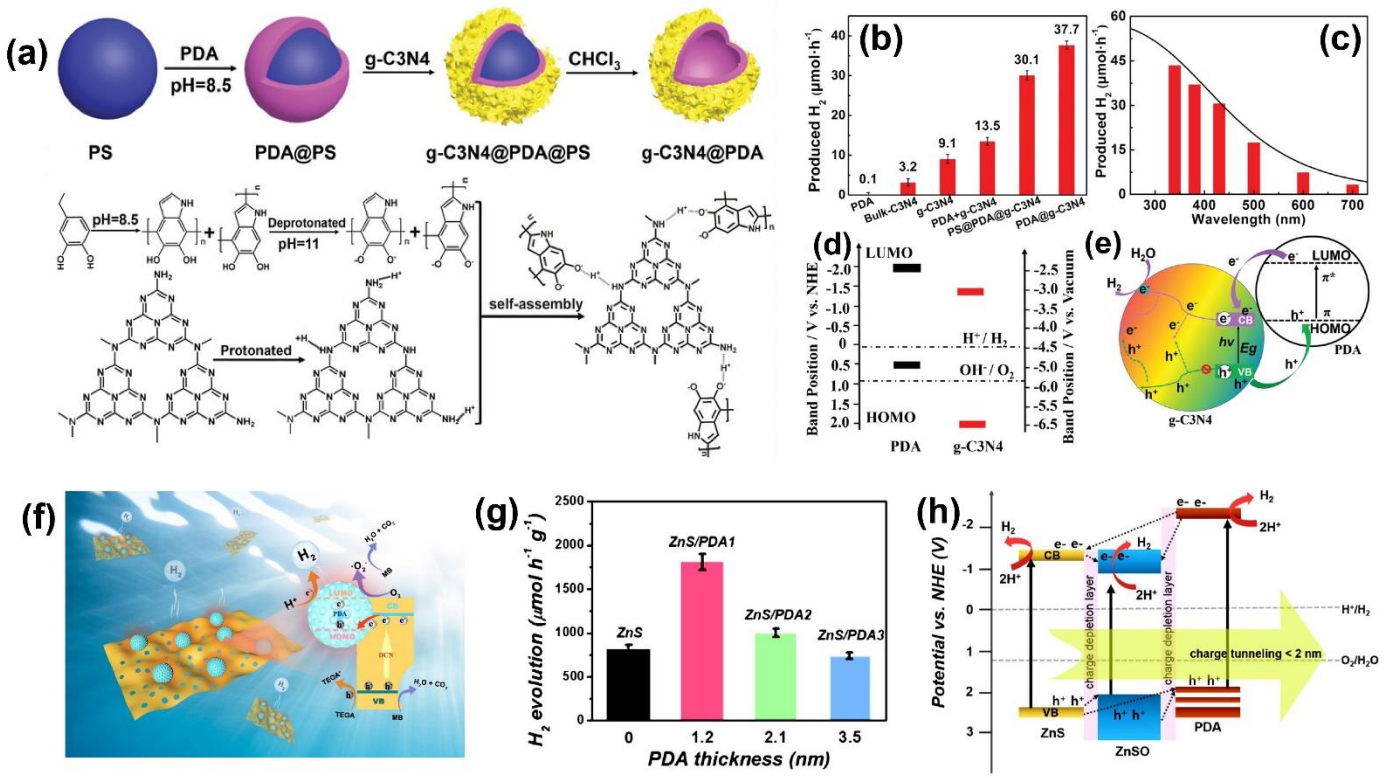

Figure 12. (**a**) The preparation process of g-C_3N_4@PDA nanosphere. (**b**) The H_2 evolution efficiency of different samples in light irradiation. (**c**) Wavelength dependence of H_2 evolution rate on g-C_3N_4@PDA photocatalyst. (**d**) Band positions of PDA and g-C_3N_4 and (**e**) electron transfer in the g-C_3N_4@PDA system (* means that the electron transuition to excited state) [144]. (**f**) Scheme diagram of PDA/DCN photocatalytic H_2 production and organic contaminant degradation [145]. (**g**) The photocatalytic H_2 production effiency under different PDA thickness. (**h**) Schematic representation of the ZnS/PDA heterojunction [94].

In addition to g-C_3N_4, transition metal sulfides, such as such as ZnS, are widely applied as an efficient photocatalyst in photocatalytic H_2 evolution, due to their high reduction potential, as well as the rapid generation of photocarriers abilities. However, the application of ZnS is hindered by photocorrosion and instability due to oxidation of sulfide ions by photogenerated holes. PDA has good adhesion and interface modification capabilities, allowing it to form uniform coatings on various material surfaces, thereby improving the surface activity and stability of the photocatalyst. Recently, nanometer-controlled PDA coatings have been shown to enhance photocatalytic activation wavelength, rather than hinder them. Kim and co-workers reported on a strongly coupled heterojunction photocatalyst comprising by a ZnS nanorod and ultrathin PDA (ZnS/PDA). Figure 12g,h shown that the highest H_2 production rate was 2162.5 μmol h^{-1} g^{-1} with PDA layer of 1.2 nm, and remained 78.7% of initial photoactivity after three cycling. In addition, since the effective carrier transmission length was limited to less than 2 nm, the excited carriers cannot be transmitted to the surface if the PDA layer was thicker than the transmission length. This research results may be applicable to other sulfonium catalyst and sensitive nanomaterials and light catalyst, such as selenide, boride, telluride, etc.

PDA has shown significant potential in the application of photocatalytic water splitting, primarily due to its unique physicochemical properties and its synergistic effects with photocatalysts. The reductive properties and excellent conductivity of PDA facilitate the transfer of photogenerated electrons and reduce the recombination of electron-hole pairs, thereby increasing the rate of hydrogen production during water splitting. Moreover, the PDA coating can be used as a protective layer to prevent photocorrosion or chemical corrosion of the catalyst, thereby improving the photocatalytic stability.

5.3. CO_2 Reduction

The burning of fossil fuels and industrial activities have increased carbon dioxide (CO_2) concentration in the atmosphere, which in turn has caused climate change and a series of environmental problems. Photocatalytic CO_2 reduction is considered a promising method for reducing carbon dioxide emissions and producing renewable fuels. It utilizes light energy to convert CO_2 into valuable chemical products, such as methanol, methane or carbon monoxide [2,146]. This process typically involves the use of a semiconductor photocatalyst, which absorbs light and generates electron-hole pairs. These carriers then participate in the reduction of CO_2 and the oxidation of a sacrificial agent or water. It is essential to use photocatalysts that can separate charge efficiently and adsorb CO_2 [147,148]. Research has shown that

the amine-functionalized metal oxides can effectively capture CO_2 by forming strong chemical adsorptive species, which not only promoted the activation of CO_2 but also enhanced the CO_2 reduction in photocatalytic.

A great deal of amino groups in PDA, can easily be anchored to most surfaces, and enhance the CO_2 adsorption and activation capacity. For example, it was demonstrated that the C_3N_4 nanospheres modified with PDA had significantly enhanced CO_2 adsorption capacity and high photocatalytic efficiency [149]. It has been reported that dopamine modification on TiO_2 nanoparticles can not only improve the charge separation efficiency, but also increase the reduction power of electrons by 100 mV [150]. In addition, compared with TiO_2 bulks, hierarchical structure of TiO_2 has a shorter distance charge transfer, thereby increasing the charge transfer, the duty carrier recombination. Meng et al. reported a series of PDA-modified TiO_2 hollow spheres (TiO_2@PDA) for photocatalytic CO_2 reduction (Figure 13a) [151]. As shown in Figure 13b, when photocatalytic CO_2 reduction reactions were performed using photocatalysts, CH_4 and CH_3OH were detected as products. For pristine TiO_2, the generating rates of CH_4 and CH_3OH were 0.30 and 0.63 μmol h^{-1} g^{-1}. With the deposition of 0.05% PDA, the CH_4 yield increased to 1.14 μmol h^{-1} g^{-1}, which was nearly four times as many as the generation rate of sample T. The higher yields and outstanding methane selectivity were contributed to the enhanced CO_2 adsorption capacity as well as efficient separation and transfer of charge carriers induced between TiO_2 and PDA (Figure 13c).

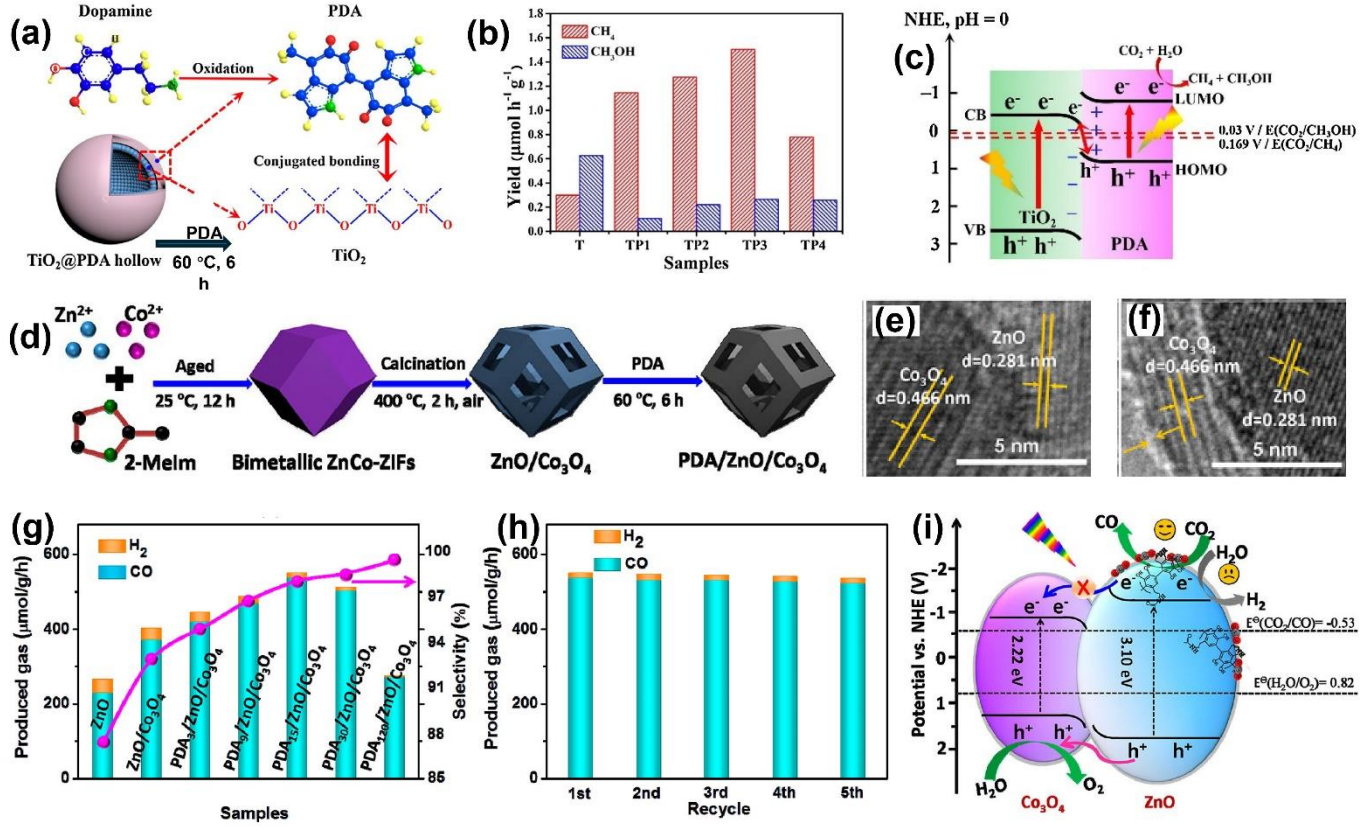

Figure 13. (**a**) Schematic illustration of TiO_2@PDA composites. (**b**) Photocatalytic yields of pure TiO_2 and TiO_2@PDA photocatalysts. (**c**) The possible mechanism of S-scheme charge transfer of TiO_2@PDA [151]. (**d**) The synthesis of PDA/ZnO/Co_3O_4 photocatalysts. (**e**,**f**) The HRTEM images of ZnO/$Co_3O_4$and PDA_{15}/ZnO/Co_3O_4. (**g**) The CO and H_2 evolution rate of different photocatalysts under UV-vis illumination (the arrow points to the CO selectivity). (**h**) The recycling performance of on PDA_{15}/ZnO/Co_3O_4. (**i**) The mechanism diagram for photocatalytic CO_2 reduction mechanism diagram via PDA_{15}/ZnO/Co_3O_4 [152].

Band position and intrinsic properties make the metal oxide can combine well matching the heterojunction formation. Additionally, the MOF-derived metal oxide also inherits the porous structure and large specific surface area, making it a promising candidate material for efficient photocatalytic CO_2 reduction [66]. For instance, a hollow ZnO/Co_3O_4 photocatalyst was constructed through pyrolyzing bimetallic ZnCo-ZIFs and modifying them with PDA (Figure 13d–f) [152]. Figure 13g shown shows the production of CO on PDA_m/ZnO/Co_3O_4, with the amount of PDA increasing from 3 mg to 120 mg. Among them, the PDA_{15}/ZnO/Co_3O_4 (the $content_{PDA}$ = 15 mg) showed the highest CO production in the photocatalytic CO_2 reduction, with a rate of 537.5 μmol/g/h and a selectivity of 97.7%. The enhanced CO_2 adsorption/activation capability was attributed to the PDA modification. Further increasing PDA to 30 mg and 120

mg resulted in a decrease in CO production, which might be attributed to the reduced light absorption by excess covering of semiconductor ZnO/Co_3O_4 surface. As a result of recycling experiments, the high photocatalytic activity and CO selectivity were maintained after five cycles (Figure 13h).

PDA shows great potential in photocatalytic CO_2 reduction through its synergistic effects with photocatalysts, particularly in enhancing photocatalytic efficiency, improving stability, and controlling product selectivity. For example, PDA combined with the amine-functionalized metal oxides can effectively capture CO_2. By optimizing the thickness and surface chemistry of PDA, it is possible to improve the selectivity of specific products.

5.4. Photocatalytic H_2O_2 Production

As an environmentally friendly oxidant and ideal carrier of energy, hydrogen peroxide (H_2O_2) has been widely used chemistries, such as chemical production, healthcare, and environmental treatment for many years [153]. As the industrial production of one of the primary methods of hydrogen peroxide, anthraquinone method is through the cycle of anthraquinone compounds REDOX reaction, high concentrations of hydrogen peroxide production. Nevertheless, the process of anthraquinone depends on precious metals and organic solvents, and consumes a lot of energy [154]. Photocatalytic H_2O_2 strategy is based on the most abundant water (H_2O) and oxygen (O_2) in nature, which uses a photocatalyst to break down water or other compounds to form hydrogen peroxide under light, is considered an emerging research direction [155,156]. Photocatalytic H_2O_2 production in the main pathways including direct photocatalytic decomposition of water oxidation reaction (WOR) and oxygen reduction reaction (ORR). Among them, ORR is considered light catalytic production of H_2O_2 main ways, where oxygen is acting as an electron acceptor. Therefore, improving the photocatalyst's ability to effectively adsorb and desorb oxygen can prevent electron-hole recombination and enhance the efficiency of photocatalytic H_2O_2 generation.

As reported that the reversible conversion between catechol and o-ben zoquinone in PDA during the photocatalytic H_2O_2 production, which was similarly to the transformation of anthraquinone. Wei et al. designed the CdS-PDA hybrid catalyst via coating PDA on CdS for H_2O_2 production (Figure 14a) [157]. The adsorption energy of O_2 on CdS (002) and CdS (002)-PDA models was estimated by performing density functional theory (DFT) calculations (Figure 14b), which was consistent with the O2TPD result in that O_2 was more strongly adsorbed on CdS (002)-PDA ($E(O_2)_{ads}$ = −2.41 eV) than that on CdS (002) ($E(O_2)_{ads}$ = −1.25 eV). The H_2O_2 selectivity of CdS -PDA was significantly enhanced from 30% to 82%, achieving a 13.7-fold catalytic yield over the CdS (Figure 14c). In addition, the K_f and K_d values (corresponding to the formation and decomposition rate constant of H_2O_2) in Figure 14d indicated that the PDA coating could not only improve the ability of O_2 adsorption, but also inhibit the decomposition of H_2O_2, and enhance the stability of CdS light corrosion. Similarly, Huang and co-workers constructed a PDA-loaded $ZnIn_2S_4$ (ZIS/PDA) for H_2O_2 production [91]. The S-scheme photocatalyst ZIS/PDA exhibited outstanding H_2O_2 production performance under visible light in pure water, where the highest H_2O_2 yield (1747 $\mu mol \cdot g^{-1} \cdot h^{-1}$), which was 39 times the yield of pure $ZnIn_2S_4$ (Figure 14e). The transition intermediates and the corresponding free energies were shown in Figure 14f, the ΔG of *OOH generated by ZIS/$PDA_{0.1}$ was much lower than that of ZIS, suggesting that the ZIS/$PDA_{0.1}$ could reduce the energy barrier and improve the overall reaction rate. The possible mechanism of photocatalytic H_2O_2 by the ZIS/$PDA_{0.1}$ was illustrated in Figure 14g. Under the influence of the internal electric field (IEF), the constructed ZIS/$PDA_{0.1}$ S scheme heterojunction rapidly separated and transfered photogenerated electrons and holes. The photogenerated electrons, which accumulated on the CB of PDA, are then consumed by oxygen and protons. The PDA coating enhanced the selectivity of H_2O_2, increased the overall reaction rate, and significantly inhibited the decomposition of H_2O_2, thereby promoting the accumulation of H_2O_2.

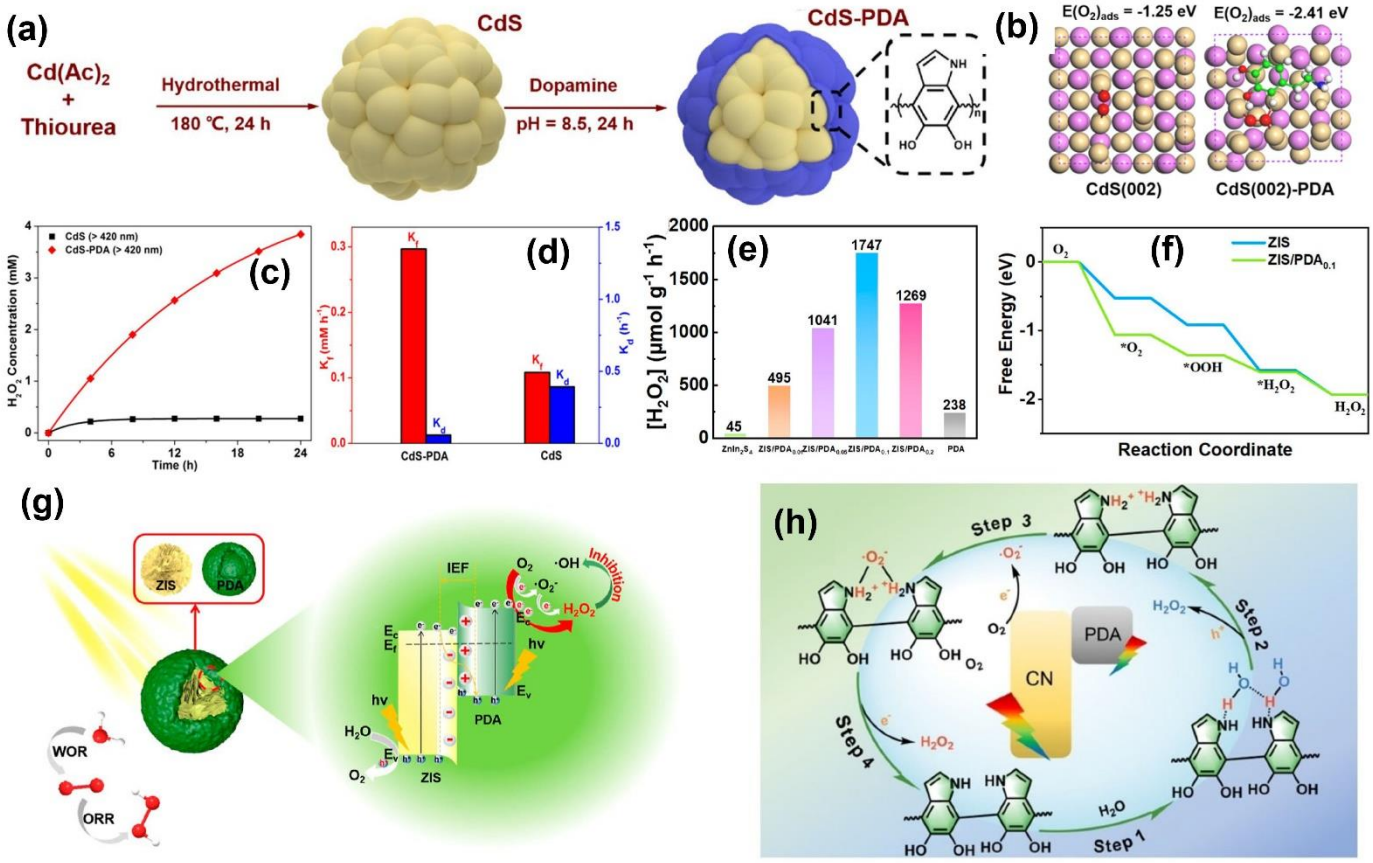

Figure 14. (**a**) The synthesis process of CdS–PDA. (**b**) Computational models for O_2 adsorption on photocatalysts. (**c**) Long-term photocatalytic H_2O_2 production and (**d**) K_f and K_d values of photocatalysts [157]. (**e**) H_2O_2 production rate of $ZnIn_2S_4$ and ZIS/PDAx. (**f**) Free energy of the intermediate state in the H_2O_2 production of ZIS and $ZIS/PDA_{0.1}$. (**g**) Mechanism of photocatalytic H_2O_2 by the sustainable transformation of $ZIS/PDA_{0.1}$ [91]. (**h**) The possible reaction mechanism of H_2O_2 production under CN-PDA [158].

In photocatalytic H_2O_2 production process, Superoxide free radical ($\bullet O_2^-$) is generated photocatalytic oxygen reduction of important intermediates, has the strong oxidizing properties, could undermine the stability of the catalyst. Therefore, avoiding the accumulation of $\bullet O_2^-$ resulting in its rapid conversion to H_2O_2 is crucial to improve catalyst stability and H_2O_2 yield. Deng et al. developed a heterojunction of PDA and g-C_3N_4 (CN-PDA) for H_2O_2 synthesis [158]. The possible mechanism of CN-PDA photocatalytic synthesis of H_2O_2 was shown in Figure 14h, which included two synthesis pathways. In WOR part, two adjacent C-NH groups on DHI absorb two water molecules. Then, $2e^-$ WOR generated H_2O_2, leaving behind two protonated amine groups (NH_2^+). On the other hand, NH_2^+ on PDA acted as a key position for the adsorption and reduction of $\bullet O_2^-$, which can rapidly convert $\bullet O_2^-$ into H_2O_2. This prevented the accumulation of $\bullet O_2^-$ that could lead to the destruction of the catalyst structure and promotes the regeneration of the C-NH group sites, thereby achieving efficient continuous production of H_2O_2.

During the photocatalytic production of hydrogen peroxide, the electrons in the conduction band react with oxygen in the solution, reducing it to O_2^-. The superoxide anion further reacts with H^+ to eventually form H_2O_2. PDA has strong adsorption capabilities, effectively capturing dissolved oxygen and inhibiting H_2O_2 decomposition. In addition, the catechol in PDA reacted with O_2 to produce H_2O_2 and obenzoquinone. Studies on the photocatalytic synthesis of hydrogen peroxide by PDA have the potential to develop green and sustainable hydrogen peroxide synthesis methods. This method can be used to produce hydrogen peroxide under environmentally friendly conditions using renewable energy sources such as sunlight and has broad application prospects.

5.5. Applications in Other Photocatalytic Reactions

5.5.1. N_2 Fixation

As an essential energy source, ammonia (NH_3) has a significant impact in industrial and agricultural production. In recent years, the photochemical synthesis of NH_3 from atmospheric nitrogen (N_2) has become a hot research frontier [159]. However, photocatalytic nitrogen fixation materials face limitations such as the difficulty of N_2 adsorption and

activation, and the challenge of preventing the recombination of photogenerated carriers [160]. PDA has shown promising application in photocatalytic nitrogen fixation due to its unique properties. Wang et al. constructed a ternary SiW_9Co_3/PDA/BWO photocatalyst, where PDA acting as an adhesive bridge between SiW_9Co_3 with BWO [161]. In this work, PDA had a broad light absorption range and acted as an electron transport chain to facilitate electron–hole migration through π–π* electronic delocalization (Figure 15a). In addition, the SiW_9Co_3/PDA/BWO provided suitable binding sites for molecular nitrogen activation due to the synergy between three photocatalysts. The catalytic efficiency of Z-scheme ternary SiW_9Co_3/PDA/BWO was 6.0 times higher than that of BWO.

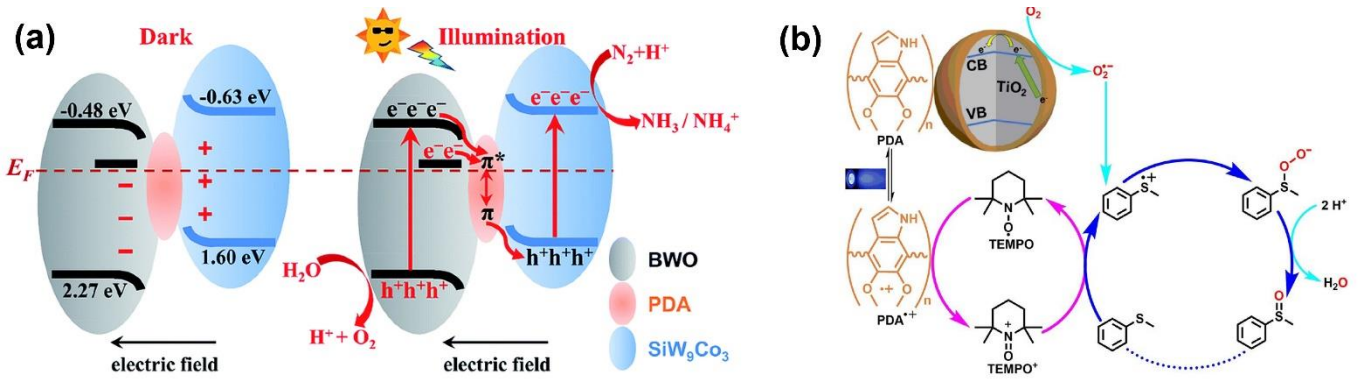

Figure 15. (**a**) Schematic illustration of separation and migration of photo-generated electron-hole pairs over the Z-scheme SiW_9Co_3/PDA/BWO heterojunction [161]. (**b**) The plausible mechanism for selective aerobic oxidation of thioanisole under visible light by combining TiO_2@PDA photocatalysis and TEMPO catalysis [162].

5.5.2. Organic Synthesis

PDA is extensively utilized in organic synthesis owing to its chemical properties and functionality. It exhibits catalytic activity and can generate active free radicals to facilitate oxidation, reduction, and coupling reactions. PDA possesses abundant surface functional groups, which allow for easy functionalization, making it an excellent substrate for developing catalysts and adsorbents. Additionally, PDA can serve as a support to immobilize metal or organic catalysts. Its functional groups can engage in reactions or alter substrate adsorption, thereby influencing reactivity. The biocompatibility of PDA also renders it particularly valuable in bioorganic synthesis, making it suitable for the synthesis of bioactive molecules or drug precursors [163–165]. Many studies have shown that PDA, as a multifunctional coating on the surface of metal oxide semiconductors, can significantly improve the photoelectric performance of these materials due to the presence of π-π* electron transitions. Shi et al. constructed the TiO_2@PDA with a large π-conjugated PDA system and used for aerobic oxidation reaction of thioanisole [162]. The possible mechanism was shown in Figure 15b, it was worth noting that PDA was activated to an unstable intermediate PDA radical$^{\bullet+}$, which can regenerate into PDA by transforming TEMPO into TEMPO$^+$. Thioanisole, under the action of TEMPO$^+$, was converted into S-centered radical cation, which prefer to react with $O_2^{\bullet-}$ to form persulfoxide. Then the persulfoxide combined with CH_3OH to yield the sulfoxide product. Hence, the strategy of surface modification of semiconductor by PDA had a great potential for photocatalytic organic transformations selectively. In addition, the synthesis of amide compounds holds great significant importance in organic synthesis. Xu and co-workers reported a magnetic Fe_3O_4/PDA/CdS active photocatalyst for the amidation of aromatic aldehydes under air, where PDA improved the photocatalytic activity by its light energy conversion [166].

In a word, PDA photocatalytic nitrogen fixation is an advanced research topic focusing on using polydopamine as a photocatalyst to convert N_2 into NH_3 under light irradiation. PDA can be used as a conductive adhesive to bridge to synthesize ternary heterojunctions with other catalysts. The PDA facilitates the separation of photogenerated electron-hole pairs from the other two semiconductors, accelerates electron transfer, and reduces recombination, which is essential for improving photocatalytic reaction efficiency. Alternatively, PDA photocatalysis system can be used to synthesize various organic compounds, possibly providing new routes to synthesize complex molecules.

6. Conclusions and Prospects

This review provides an in-depth discussion on the structural characteristics and synthesis methods of polydopamine (PDA). It highlights PDA's advantages in photocatalytic applications, such as its templating agent effect, light absorption performance, film-forming ability, hydrophilicity, and conductivity. The article also addresses strategies for

enhancing PDA's photocatalytic performance and explores the application of PDA-based materials in various fields, including solar water purification (targeting heavy metal reduction, organic pollutant degradation, and antibacterial activity), H_2 production, H_2O_2 production, CO_2 reduction, and organic transformation. The ultimate goal of the review is to offer valuable insights for the design and development of PDA-based photocatalytic materials. While PDA holds significant promise in the field of photocatalysis, it also faces certain challenges that need to be addressed.

(1) To address the complexity of the PDA synthesis process and the difficulty of functionalization, the following strategies can be used to improve the process: simplified synthesis methods, such as one-step synthesis and direct oxidation, as well as the use of microwave-assisted synthesis to accelerate the reaction; simplified methods of functionalization, including the use of pre-functionalized dopamine precursors and in-situ functionalization techniques; highly efficient methods of functionalization, such as surface self-assembly and cross-linking functionalization; green synthesis methods, such as bio templating and enzymatic polymerization; and template-assisted synthesis, including hard and soft template methods, to control the morphology and structure of PDA. These strategies help to improve the preparation efficiency and performance of PDA and enhance their maneuverability and economy in practical applications.

(2) To improve the limited light absorption range and weak absorption capacity of PDA, it can be improved by various strategies to enhance its potential for photocatalytic applications. These strategies include: doping of metallic or nonmetallic elements to modulate the energy band structure and electronic structure; dye sensitization (e.g., phthalocyanine and porphyrin dyes) to broaden the light absorption range; construction of composites of PDA with other inorganic semiconductors to fabricate heterojunctions to improve light absorption capacity; surface modification and functionalization to introduce conjugated groups (e.g., benzene rings, alkynyl groups, etc.) or grafting of photosensitizing compounds to change the light absorption properties; design of different nanostructures such as nanoparticles and porous structures to improve light absorption efficiency; and other approaches such as composite with surface plasmon resonance effect materials and copolymer design. Together, these approaches can help to enhance the effectiveness of PDA in applications, such as environmental remediation and energy conversion.

(3) To solve the problem of high PDA photogenerated carrier complexation rate, various strategies can be adopted, including metallic or nonmetallic doping to modulate the energy band structure and promote carrier separation, dye sensitization to enhance light absorption and assist in carrier separation, construction of heterojunctions to promote the transfer of electrons and holes, surface modification and functionalization to change the electronic structure, design of novel nanostructures to increase the carrier transport path, composite with surface plasmon resonance effect materials to enhance the electromagnetic field and promote carrier separation, optimization of synthesis methods to improve the electronic structure of the materials, application of external electric or magnetic fields to guide the directional movement of carriers, and optimization of photocatalytic reaction conditions to promote carrier separation. The combined application of these methods can significantly reduce the photogenerated carrier complexation rate in PDAs and enhance the photocatalytic efficiency.

(4) To enhance the stability of PDA, the reaction conditions can be adjusted to optimize the pH to a weakly basic range and synthesize at low temperature to reduce the occurrence of side reactions; doping with metallic or non-metallic elements to enhance the stability; surface modification to reduce hydrolysis and degradation through the introduction of hydrophobic groups; the use of chemical cross-linking agents to form a stable three-dimensional network structure; designing the nanostructures of PDA, such as nanoparticles and porous structures, to enhance stability; optimization of the synthesis process such as shortening the reaction time and adjusting the stirring speed to reduce side reactions and improve the homogeneity of the reaction. The implementation of these strategies helps to improve the stability of PDA, which in turn provides better performance and wider application prospects in areas such as photocatalysis and environmental remediation.

(5) PDA holds significant potential in the field of environmental remediation and energy conversion due to its unique chemical properties and biocompatibility. For instance, (a): PDA combined with sporous materials can serve as support materials for photocatalysts, enhancing their stability and recyclability. Its excellent adsorption properties allow it to effectively capture pollutants in water, such as organic dyes and heavy metal ions, facilitating their degradation under light irradiation; (b): In the process of water splitting for hydrogen production, PDA can act as a co-catalyst, promoting the separation of photogenerated electrons and holes, thereby enhancing hydrogen production efficiency. (c): PDA also has potential applications in the photocatalytic reduction of CO_2. It can interact with CO_2 molecules, increasing their adsorption on the photocatalyst surface, which facilitates the reduction reaction and improves the selectivity and efficiency of the process; (d): Leveraging PDA's photocatalytic properties,

self-cleaning and antimicrobial coatings can be developed. When exposed to light, PDA coatings can catalyze the degradation of organic pollutants and bacteria, maintaining surface cleanliness. This application is particularly promising in building materials, medical devices, and textiles; (e) The excellent biocompatibility, tunable photothermal conversion performance, and extensive surface modification ability make PDA become a potential material in the fields of biomedicine (photothermal therapy, antibacterial applications), energy (energy storage), and environmental science (solar-driven evaporation and desalination).

In summary, improving the comprehensive performance of PDA includes the use of simplified synthesis, functionalization strategies, doping, sensitization, surface and nanostructure design to enhance their preparation efficiency, light absorption ability and photocatalytic potential. Meanwhile, the stability of PDA can be effectively enhanced by adjusting the reaction conditions, doping, surface modification, cross-linking, nano structuring, and synthesis process, thus expanding its application in photocatalysis.

Acknowledgments

The authors would like to thank Canada First Research Excellence Fund (CFREF) and Natural Sciences and Engineering Research Council of Canada-Discovery Grant for their funding. H.W. acknowledges the financial support from the China Scholarship Council.

Author Contributions

H.W.: Writing–original draft, Supervision, Formal analysis. L.J.: Writing–review & editing, Supervision. A.V.: Supervision. Y.Y.: Supervision. H.Z.: Supervision. Q.G.: Supervision. J.H.: Writing–review& editing, Supervision, Funding acquisition.

Ethics Statement

Not applicable.

Informed Consent Statement

Not applicable.

Funding

This research was funded by Natural Sciences and Engineering Research Council of Canada, Discovery Grant [grant number: 10040079].

Declaration of Competing Interest

The authors declare that they have no known competing financial interests or personal relationships that could have appeared to influence the work reported in this paper.

References

1. Kumari H, Sonia, Suman, Ranga R, Chahal S, Devi S, et al. A review on photocatalysis used for wastewater treatment: Dye degradation. *Water Air Soil Pollut.* **2023**, *234*, 349.
2. Fang S, Rahaman M, Bharti J, Reisner E, Robert M, Ozin GA, et al. Photocatalytic CO_2 reduction. *Nat. Rev. Method Prime* **2023**, *3*, 61.
3. Cao W, Zhang W, Dong L, Ma Z, Xu J, Gu X, et al. Progress on quantum dot photocatalysts for biomass valorization. *Exploration* **2023**, *3*, 20220169.
4. Kong Y, Yang C, Cai Y, Mu X, Li L. Photocatalytic aerobic conversion of methane. *Photocatal. Res. Potential* **2023**, *1*, 10005.
5. Huang Z, Luo N, Zhang C, Wang F. Radical generation and fate control for photocatalytic biomass conversion. *Nat. Rev. Chem.* **2022**, *6*, 197–214.
6. Wang J, Wang X, Zhao H, Van Humbeck JF, Richtik BN, Dolgos MR, et al. Selective C3–C4 cleavage via glucose photoreforming under the effect of nucleophilic dimethyl sulfoxide. *ACS Catal.* **2022**, *12*, 14418–14428.
7. Wang J, Zhao H, Chen L, Björk J, Rosen J, Kumar P, et al. Selective cellobiose photoreforming for simultaneous gluconic acid and syngas production in acidic conditions. *Appl. Catal. B Environ.* **2024**, *344*, 123665.

8. Yang P, Zhu F, Zhang Z, Cheng Y, Wang Z, Li Y. Stimuli-responsive polydopamine-based smart materials. *Chem. Soc. Rev.* **2021**, *50*, 8319–8343.
9. Aguilar-Ferrer D, Szewczyk J, Coy E. Recent developments in polydopamine-based photocatalytic nanocomposites for energy production: Physico-chemical properties and perspectives. *Catal. Today* **2022**, *397–399*, 316–349.
10. Zhu X, Chen C, Shi Y, Wang J, Wang Y, Pan L, et al. Dual-functional, highly efficient $CaIn_2S_4$/PDA@SnO_2 photocatalyst with Z-Scheme for photocatalytic hydrogen production from water splitting and organic pollutant degradation. *J. Alloys Compd.* **2024**, *976*, 173151.
11. Han G, Xu F, Cheng B, Li Y, Yu J, Zhang L. Enhanced photocatalytic H_2O_2 production over inverse opal ZnO@Polydopamine S-scheme heterojunctions. *Acta Phys. Chim. Sin.* **2022**, *38*, 2112037.
12. Zhang X, Yu J, Macyk W, Wageh S, Al-Ghamdi AA, Wang L. C_3N_4/PDA S-Scheme heterojunction with enhanced photocatalytic H_2O_2 production performance and its mechanism. *Adv. Sustain. Syst.* **2022**, *7*, 2200113.
13. Feng S, Wang S, Lei C, Liu S, Jin Q. Photocatalytic degradation of antibiotics by S-Scheme heterojunctions constructed by thermally sheared flower-like TiO_2-loaded PDA. *Catal. Lett.* **2023**, *153*, 3783–3794.
14. da Silva AFV, da Silva J, Vicente R, Ambrosi A, Zin G, Di Luccio M, et al. Recent advances in surface modification using polydopamine for the development of photocatalytic membranes for oily wastewater treatment. *J. Water Process Eng.* **2023**, *53*, 103743.
15. Yang D, Wang W, Zhao X, Zhou Z, Ren H, Chen Y, et al. Synthesis of high-efficient g-C_3N_4/polydopamine/CdS nanophotocatalyst based on bioinspired adhesion and chelation. *Mater. Res. Bull.* **2020**, *131*, 110970.
16. Bernsmann F, Ball V, Addiego F, Ponche A, Michel M, Gracio JJ, et al. Dopamine-melanin film deposition depends on the used oxidant and buffer solution. *Langmuir* **2011**, *27*, 2819–2825.
17. Liu Y, Ai K, Lu L. Polydopamine and its derivative materials: Synthesis and promising applications in energy, environmental, and biomedical fields. *Chem. Rev.* **2014**, *114*, 5057–5115.
18. Hong S, Na YS, Choi S, Song IT, Kim WY, Lee H. Non-covalent self-assembly and covalent polymerization Co-contribute to polydopamine formation. *Adv. Funct. Mater.* **2012**, *22*, 4711–4717.
19. Li M, Xuan Y, Zhang W, Zhang S, An J. Polydopamine-containing nano-systems for cancer multi-mode diagnoses and therapies: A review. *Int. J. Biol. Macromol.* **2023**, *247*, 125826.
20. Zou Y, Chen X, Yang P, Liang G, Yang Y, Gu Z, et al. Regulating the absorption spectrum of polydopamine. *Sci. Adv.* **2020**, *6*, eabb4696.
21. Bai W, Yang P, Liu H, Zou Y, Wang X, Yang Y, et al. Boosting the optical absorption of melanin-like polymers. *Macromolecules* **2022**, *55*, 3493–3501.
22. Dong W, Zhao Z, Liu F, Li P, Wang L, Zhou Y, et al. PVDF nanofiber modified with ZnO nanowires/polydopamine for the treatment of sewage containing heavy metals, organic dyes, and bacteria. *ACS Appl. Mater. Interfaces* **2023**, *15*, 58994–59004.
23. Sun X, Yan L, Xu R, Xu M, Zhu Y. Surface modification of TiO_2 with polydopamine and its effect on photocatalytic degradation mechanism. *Colloids Surf. A* **2019**, *570*, 199–209.
24. Nie N, He F, Zhang L, Cheng B. Direct Z-scheme PDA-modified ZnO hierarchical microspheres with enhanced photocatalytic CO_2 reduction performance. *Appl. Surf. Sci.* **2018**, *457*, 1096–1102.
25. Yu Z, Li F, Yang Q, Shi H, Chen Q, Xu M. Nature-mimic method to fabricate polydopamine/graphitic carbon nitride for enhancing photocatalytic degradation performance. *ACS Sustain. Chem. Eng.* **2017**, *5*, 7840–7850.
26. Gao J, He Q, Liang G, Luo L, Liu X, Cai K, et al. Heterogeneous alloyed CuSnO-DopaCube mediated photo-Fenton and photothermal synergistic catalysis for dye elimination. *J. Alloys Compd.* **2023**, *960*, 170737.
27. Shen Z, Wang X, Fan D, Xu X, Lu Y. Wood–hydrogel composites coated with C_3N_4 photocatalyst for synchronous solar steam generation and photocatalytic degradation. *J. Mater. Sci.* **2023**, *58*, 13154–13164.
28. Usta DD, Celebi N, Soysal F, Saglam ASY, Yildiz N, Salimi K. Bio-inspired NIR responsive Au-pDA@pDA sandwich nanostructures with excellent photo-thermal performance and stability. *Colloids Surf. A* **2021**, *611*, 125758.
29. Zhao X, Zha X, Tang L, Pu J, Ke K, Bao R.-Y, et al. Self-assembled core-shell polydopamine@MXene with synergistic solar absorption capability for highly efficient solar-to-vapor generation. *Nano Res.* **2020**, *13*, 255–264.
30. Lu Y, Fan D, Shen Z, Zhang H, Xu H, Yang X. Design and performance boost of a MOF-functionalized-wood solar evaporator through tuning the hydrogen-bonding interactions. *Nano Energy* **2022**, *95*, 107016.
31. Pang AL, Arsad A, Ahmad Zaini MA, Garg R, Saqlain Iqbal M, Pal U, et al. A comprehensive review on photocatalytic removal of heavy metal ions by polyaniline-based nanocomposites. *Chem. Eng. Commun.* **2023**, *211*, 275–299.
32. Jamali Alyani S, Dadvand Koohi A, Ashraf Talesh SS, Ebrahimian Pirbazari A. Investigation of TiO_2/PPy nanocomposite for photocatalytic applications; synthesis, characterization, and combination with various substrates: A review. *Environ. Sci. Pollut. Res. Int.* **2024**, *31*, 42521–42546.
33. Yang Y, Cao Z, Shen T, Zhang J, Gu Z, Zhao M, et al. Synergistic photocatalytic-photothermal contribution induced by Pd-TiO_2/PEDOT immobilized in PVDF membrane for enhanced water purification. *Chem. Eng. J.* **2024**, *494*, 153168.
34. Jasemizad T, Malmström J, Padhye LP. Mechanistic investigation of the photocatalytic activity of PEDOT for aqueous contaminant removal: The role of iron and hydroxyl radicals. *Environ. Sci. Wat. Res.* **2024**, *10*, 1256–1270.

35. Dey S, Manna K, Pradhan P, Sarkar AN, Roy A, Pal S. Review of polymeric nanocomposites for photocatalytic wastewater treatment. *ACS Appl. Nano Mater.* **2024**, *7*, 4588–4614.
36. Barclay TG, Hegab HM, Clarke SR, Ginic-Markovic M. Versatile surface modification using polydopamine and related polycatecholamines: Chemistry, structure, and applications. *Adv. Mater. Interfaces* **2017**, *4*, 1601192.
37. Wang W, Dong X, Huang X, Wu H, Zhu D. Polydopamine-mediated CdS crystal growth behavior and the synergistic photocatalytic–adsorption mechanisms in removing Rhodamine B. *Energ. Fuels* **2023**, *37*, 18184–18193.
38. Ryu JH, Messersmith PB, Lee H. Polydopamine surface chemistry: A decade of discovery. *ACS Appl. Mater. Interfaces* **2018**, *10*, 7523–7540.
39. Shi J, Zhang J, Jia Z, Zhao R, Abubakr Yasin UA, Du J. Construction of yolk-shell structural polydopamine@WO_3 micro/nanospheres for enhanced photocatalytic degradation. *ChemistrySelect* **2023**, *8*, e202301084.
40. Qin Y, Xu L, Zhu Z, Wong W-Y. Strongly coupled interface facilitating charge separation to the improved visible light-driven hydrogen production on CdS@polydopamine/NiS photocatalyst. *J. Mater. Chem. A* **2023**, *11*, 11840–11848.
41. Qu R, Zhang W, Liu N, Zhang Q, Liu Y, Li X, et al. Antioil Ag_3PO_4 nanoparticle/polydopamine/Al_2O_3 sandwich structure for complex wastewater treatment: Dynamic catalysis under natural light. *ACS Sustain. Chem. Eng.* **2018**, *6*, 8019–8028.
42. Zhong J, Xiao F, Jin B, Zhang G, Hou H, Bi J, et al. Construction of sandwich-structured V_2CT_x@PDA@Ag nanosheet composite for enhanced near-infrared photothermocatalytic sterilization performance. *Mater. Chem. Phys.* **2024**, *314*, 128931.
43. Shang L, Li W, Wang X, Ma L, Li L, Duan Q, et al. Preparation of magnetic Fe_3O_4@PDA/CuS core-shell nanocomposite as a green photocatalyst. *Synth. Met.* **2023**, *292*, 117230.
44. Inoue A, Yuk H, Lu B, Zhao X. Strong adhesion of wet conducting polymers on diverse substrates. *Sci. Adv.* **2020**, *6*, eaay5394.
45. Beygisangchin M, Abdul Rashid S, Shafie S, Sadrolhosseini AR, Lim HN. Preparations, properties, and applications of polyaniline and polyaniline thin films-a review. *Polymers* **2021**, *13*, 2003.
46. Wen J, Li X, Zhang H, Zheng S, Yi C, Yang L, et al. Architecting Janus hydrogel evaporator with polydopamine-TiO_2 photocatalyst for high-efficient solar desalination and purification. *Sep. Purif. Technol.* **2023**, *304*, 122403.
47. Feng X, Liu C, Long R, Liu S, Liu X. Polydopamine-modified magnetic foam composites synergistically activate peroxymonosulfate with visible light for sulfadiazine degradation and oil–water separation. *Chem. Eng. J.* **2023**, *478*, 147252.
48. Chen X, Ma H, Ji X, Han R, Pang K, Yang Z, et al. Engineering green MOF-based superhydrophobic sponge for efficiently synchronous removal of microplastics and pesticides from high-salinity water. *Water Res.* **2023**, *243*, 120314.
49. Duan J, Fang X, Li C, Qu J, Guo L, Zou Y, et al. Efficient and stable monolithic microreactor with Ag/AgCl photocatalysts coated on polydopamine modified melamine sponge for photocatalytic water purification. *Colloids Surf. A* **2023**, *659*, 130759.
50. Ran J, Bi S, Jiang H, Telegin F, Bai X, Yang H, et al. Core–shell $BiVO_4$@PDA composite photocatalysts on cotton fabrics for highly efficient photodegradation under visible light. *Cellulose* **2019**, *26*, 6259–6273.
51. Ran J, Chen H, Bai X, Bi S, Jiang H, Cai G, et al. Immobilizing CuO/$BiVO_4$ nanocomposite on PDA-templated cotton fabric for visible light photocatalysis, antimicrobial activity and UV protection. *Appl. Surf. Sci.* **2019**, *493*, 1167–1176.
52. Zhao J, Chen J, Chen Z, Zhang Y, Xia D, Wang Q. Flexible cotton fabrics/PDA/BiOBr composite photocatalyst using bioinspired polydopamine as electron transfer mediators for dye degradation and Cr(VI) reduction under visible light. *Colloids Surf. A* **2020**, *593*, 124623.
53. Fan G, Ning R, Li X, Lin X, Du B, Luo J, et al. Mussel-inspired immobilization of photocatalysts with synergistic photocatalytic-photothermal performance for water remediation. *ACS Appl. Mater. Interfaces* **2021**, *13*, 31066–31076.
54. Zhou J, Zhao Z, Wang Y, Ding Z, Xu X, Peng W, et al. $BiOCl_{0.875}Br_{0.125}$/polydopamine functionalized PVDF membrane for highly efficient visible-light-driven photocatalytic degradation of roxarsone and simultaneous arsenic immobilization. *Chem. Eng. J.* **2020**, *402*, 126048.
55. Shi Y, Chen X, Wu Q, Zhen H, Wang S, Dong H, et al. Enhance organic pollutants removal of wastewater by a PVDF/PDA-TiO_2 composite membrane with photocatalytic property. *J. Environ. Chem. Eng.* **2023**, *11*, 110389.
56. Wang B, Cao Q, Cheng M, Li G, Zhang J, Jiang H. Photocatalytic degradation of antibiotics in water by pollution-free photocatalytic films with a three-dimensional layered structure and the reaction mechanism study. *J. Water Process Eng.* **2023**, *52*, 103550.
57. Huang Z, Zeng Q, Hui Y, Alahi MEE, Qin S, Wu T. Fast polymerization of polydopamine based on titanium dioxide for high-performance flexible electrodes. *ACS Appl. Mater. Interfaces* **2020**, *12*, 14495–14506.
58. Zhou Z, Yang D, Wang W, Chen Y, Zhao Z, An K, et al. Bioinspired construction of g-C_3N_4 nanolayers on a carbonized polydopamine nanosphere surface with excellent photocatalytic performance. *Ind. Eng. Chem. Res.* **2020**, *59*, 12389–12398.
59. Li Y, He Z, Liu L, Jiang Y, Ong W-J, Duan Y, et al. Inside-and-out modification of graphitic carbon nitride (g-C_3N_4) photocatalysts via defect engineering for energy and environmental science. *Nano Energy* **2023**, *105*, 108032.
60. Huo R, Yang X-L, Yang J-Y, Yang S-Y, Xu Y-H. Self-assembly synthesis of $BiVO_4$/Polydopamine/g-C_3N_4 with enhanced visible light photocatalytic performance. *Mater. Res. Bull.* **2018**, *98*, 225–230.
61. Li X, Yu Z, Shao L, Zeng H, Liu Y, Feng X. A novel strategy to construct a visible-light-driven Z-scheme (ZnAl-LDH with active phase/g-C_3N_4) heterojunction catalyst via polydopamine bridge (a similar “bridge” structure). *J. Hazard. Mater.* **2020**, *386*, 121650.

62. Guo F, Chen J, Zhao J, Chen Z, Xia D, Zhan Z, et al. Z-scheme heterojunction g-C_3N_4@PDA/BiOBr with biomimetic polydopamine as electron transfer mediators for enhanced visible-light driven degradation of sulfamethoxazole. *Chem. Eng. J.* **2020**, *386*, 124014.
63. Lam Y, Fan S, He L, Ho Y, Fei B, Xin JH. Charge-controllable mussel-inspired magnetic nanocomposites for selective dye adsorption and separation. *Chemosphere* **2022**, *300*, 134404.
64. Wu C, Zuo H, Zhang S, Zhao S, Du H, Yan Q. A novel strategy to construct a direct Z-Scheme Bi@$Bi_2O_2CO_3$/g-C_3N_4 heterojunction catalyst via PDA electronic bridge. *Sep. Purif. Technol.* **2022**, *294*, 121242.
65. Liu X, Zhang T, Li Y, Zhang J, Du Y, Yang Y, et al. CdS@Polydopamine@SnO_{2-x} sandwich structure with electrostatic repulsion effect and oxygen deficiency: Enhanced photocatalytic hydrogen evolution activity and inhibited photo-corrosion. *Chem. Eng. J.* **2022**, *434*, 134602.
66. Gautam S, Agrawal H, Thakur M, Akbari A, Sharda H, Kaur R, et al. Metal oxides and metal organic frameworks for the photocatalytic degradation: A review. *J. Environ. Chem. Eng.* **2020**, *8*, 103726.
67. Majeed AH, Mohammed LA, Hammoodi OG, Sehgal S, Alheety MA, Saxena KK, et al. A review on polyaniline: Synthesis, properties, nanocomposites, and electrochemical applications. *Int. J. Polym. Sci.* **2022**, *2022*, 9047554.
68. Pang AL, Arsad A, Ahmadipour M. Synthesis and factor affecting on the conductivity of polypyrrole: A short review. *Polym. Advan. Technol.* **2020**, *32*, 1428–1454.
69. Li L, Chi L, Zhang H, Wu S, Wang H, Luo Z, et al. Fabrication of Ti-PDA nanoparticles with enhanced absorption and photocatalytic activities for hexavalent chromium Cr(VI) removal. *Appl. Surf. Sci.* **2022**, *580*, 152168.
70. Li W, Shang L, You D, Li H, Wang H, Ma L, et al. Fabrication of Fe_3O_4@Ti-PDA nanoparticles with enhanced photocatalytic activities for degradation of organic dye. *J. Phys. Chem. Solids* **2023**, *172*, 111047.
71. Wang H, Yan R, Zou Y, Xing D, Zhong K. Light-driven self-healing polyurethane based on PDA@ Ag nanoparticles with improved mechanical and antibacterial properties. *J. Mater. Chem. B* **2022,** *10*, 1085–1093.
72. Hou X, Cai Y, Song X, Wu Y, Zhang J, Wei Q. Electrospun TiO_2 nanofibers coated with polydopamine for enhanced sunlight-driven photocatalytic degradation of cationic dyes. *Surf. Interface Anal.* **2019**, *51*, 169–176.
73. Han D, Li Y, Liu X, Yeung KWK, Zheng Y, Cui Z, et al. Photothermy-strengthened photocatalytic activity of polydopamine-modified metal-organic frameworks for rapid therapy of bacteria-infected wounds. *J. Mater. Sci. Technol.* **2021**, *62*, 83–95.
74. Wang W, Li M, Huang X, Fang J, Peng F, Huang H. Structural evolution mechanisms of Polydopamine/CdS and photothermal effect boosted photocatalytic H_2 production activity. *Appl. Surf. Sci.* **2022**, *601*, 154114.
75. Mei H, Gao Z, Wang Q, Sun H, Zhao K, Zhang P, et al. Ultrasound expands the versatility of polydopamine coatings. *Ultrason. Sonochem.* **2021**, *74*, 105571.
76. Gong Z, Chen L, Chen K, Gou S, Zhao X, Song L, et al. Significantly improved photocatalytic H_2O_2 generation over PDA-modified g-C_3N_4 via promoting charge-carriers separation and oxygen adsorption. *J. Environ. Chem. Eng.* **2023**, *11*, 109405.
77. Li Y, Wei W, Guo Z, Zou L, Li M, Ai L, et al. Double-sided assembly of 0D polydopamine on 1D hexagonal tubular carbon nitride for boosting photocatalytic Cr(VI) reduction. *Sep. Purif. Technol.* **2022**, *299*, 121730.
78. Chu J, Li W, Cao Z, Bai X, Rao X, Zheng S, et al. Benzene bridged carbon nitride for efficient photocatalytic hydrogen evolution. *Photocatal. Res. Potential* **2024**, *1*, 10001.
79. Zhang H, Zhao H, Zhai S, Zhao R, Wang J, Cheng X, et al. Electron-enriched Lewis acid-base sites on red carbon nitride for simultaneous hydrogen production and glucose isomerization. *Appl. Catal. B Environ.* **2022**, *316*, 121647.
80. Chen Y, Dong S, Zhang H, Wei Y, Wang B, Zhang Y. Boosting electron transfer in Cu_2O@PDA hollow fiber membranes to decompose oxytetracycline under visible light with persulfate. *Sep. Purif. Technol.* **2023**, *318*, 124024.
81. Chen F, Zhao L, Yu W, Wang Y, Zhang H, Guo L-H. Dynamic monitoring and regulation of pentachlorophenol photodegradation process by chemiluminescence and TiO_2/PDA. *J. Hazard. Mater.* **2020**, *399*, 123073.
82. Sridharan M, Kamaraj P, Vennila R, Huh YS, Arthanareeswari M. Bio-inspired construction of melanin-like polydopamine-coated CeO_2 as a high-performance visible-light-driven photocatalyst for hydrogen production. *New J. Chem.* **2020**, *44*, 15223–15234.
83. Chen F, Yu W, Qie Y, Zhao L, Zhang H, Guo L-H. Enhanced photocatalytic removal of hexavalent chromium through localized electrons in polydopamine-modified TiO_2 under visible irradiation. *Chem. Eng. J.* **2019**, *373*, 58–67.
84. Zhou X, Jin B, Luo J, Gu X, Zhang S. Photoreduction preparation of Cu_2O@polydopamine nanospheres with enhanced photocatalytic activity under visible light irradiation. *J. Solid State Chem.* **2017**, *254*, 55–61.
85. Yang F, Wang F, Guo, Z. Characteristics of binary WO_3@ CuO and ternary WO_3@ PDA@ CuO based on impressive sensing acetone odor. *J. Colloid Interface Sci.* **2018,** *524*, 32–41.
86. Zhao R, Zhang H, Zhao R, Liu W, Liu Q, Hu H. Dynamic Cu(I)/Cu(II) redox shuttle for maltose and lactose isomerization under pulsed electric field. *ACS Sustain. Chem. Eng.* **2024**, *12*, 6232–6241.
87. Chilivery R, Zhang R, Chen G, Yao D, Fan D, Lu F, et al. Facile in situ construction of novel hybrid 3D-BiOCl@PDA heterostructures with vacancy induced charge transfer for efficient visible light driven photocatalysis and antibacterial activity. *Colloids Surf. A* **2023**, *656*, 130415.

88. Huang X, Niu Y, Peng Z, Hu W. Core–shell structured BiOCl@polydopamine hierarchical hollow microsphere for highly efficient photocatalysis. *Colloids Surf. A* **2019**, *580*, 123747.
89. Ren H-T, Jing M-Z, Li D-S, Li T-T, Lou C-W, Lin J-H, et al. Photocatalytic reduction of Cr(VI) by $Bi_{2.15}WO_6$ complexed with polydopamine: Contribution of the ligand-to-metal charge transfer path. *J. Colloid Interface Sci.* **2022**, *622*, 50–61.
90. Zhao X, Zhang N, Yu Y, Fang T, Hu J, Feng J, et al. Exploring $Bi_4V_2O_{11}$ as photoanode for water splitting with a wide range of solar light capture and suitable band potential. *Photocatal. Res. Potential* **2023**, *1*, 10002.
91. Huang S, Gao J, Zhou L, Lei J, Wang L, Liu Y, et al. Polydopamine-loaded $ZnIn_2S_4$ photocatalyst for H_2O_2 production in water. *ACS Appl. Nano Mater.* **2024**, *7*, 4481–4490.
92. Feng C, Zhang L. Microdroplet assisted hollow ZnCdS@ PDA nanocages' synergistic confinement effect for promoting photocatalytic H_2O_2 production. *Mater. Horiz.* **2024**, *11*, 1515–1527.
93. Lu J, Fang C, Wang G, Zhu L. Design of one-Dimensional cadmium sulfide/polydopamine heteronanotube photocatalysts for ultrafast degradation of antibiotics. *Ind. Eng. Chem. Res.* **2022**, *61*, 1100–1110.
94. Kim Y, Coy E, Kim H, Mrówczyński R, Torruella P, Jeong D-W, et al. Efficient photocatalytic production of hydrogen by exploiting the polydopamine-semiconductor interface. *Appl. Catal. B Environ.* **2021**, *280*, 119423.
95. Meng S, Zeng W, Wang M, Niu L, Hu S, Su B, et al. Nature-mimic fabricated polydopamine/MIL-53 (Fe): Efficient visible-light responsive photocatalysts for the selective oxidation of alcohols. *New J. Chem.* **2020**, *44*, 2102–2110.
96. Celebi N, Aydin MY, Soysal F, Yıldız N, Salimi K. Core/shell PDA@UiO-66 metal–organic framework nanoparticles for efficient visible-light photodegradation of organic dyes. *ACS Appl. Nano Mater.* **2020**, *3*, 11543–11554.
97. Huang H, Hou L, Du H, Wei H, Liu X, Wang Q, et al. Efficient dual defense: PDA-Cu coating for simultaneous corrosion resistance and antibacterial protection of Mg alloys. *Corros. Sci.* **2024**, *233*, 112103.
98. Tan L, Zhu T, Huang Y, Yuan H, Shi L, Zhu Z, et al. Ozone-induced rapid and green synthesis of polydopamine coatings with high uniformity and enhanced stability. *Adv. Sci.* **2024**, *11*, e2308153.
99. Hu S, Du H, Huang H, Wei Y, Hou L, Wang Q, et al. Deposition of modifiable MAO-PDA coatings on magnesium alloy based on photocatalytic effect. *Appl. Surf. Sci.* **2024**, *669*, 160522.
100. Zhang HD, Chen AY, Gan B, Jiang H, Gu LJ. Corrosion protection investigations of carbon dots and polydopamine composite coating on magnesium alloy. *J. Magnes. Alloy* **2022**, *10*, 1358–1367.
101. Gao J, Cheng S, Zhou P, Zhang J, Li H, Zhang Y, et al. Fenton-driven photothermal enhanced degradation of methylene blue by using Cu_2O@SnO_2@PDA cubic heterostructured catalyst. *Mater. Lett.* **2023**, *334*, 133724.
102. Wen L, Wanpei H, Qian L, Xu L, Rongsheng C, Hongwei N, et al. Antibacterial properties of Ag/TiO_2/PDA nanofilm on anodized 316L stainless steel substrate under illumination by a normal flashlight. *J. Mater. Sci.* **2020**, *55*, 9538–9550.
103. Jiang J, Chen Z, Wang P, Gu P-Y, Liu J, Zhang Z, et al. Preparation of black hollow TiO_2 nanotube-coated PDA@Ag_2S heterostructures for efficient photocatalytic reduction of Cr(VI). *J. Solid State Chem.* **2022**, *307*, 122865.
104. Chen F, Yu W, Wang Y, Wang S, Liang Y, Wang L, et al. Dynamic control of pentachlorophenol photodegradation process using P25/PDA/BiOBr through regulation of photo-induced active substances and chemiluminescence. *Chemosphere* **2022**, *307*, 135914.
105. Zhang Z, Li M, Wang H. ZIF-8 derived ZnO decorated with polydopamine and Au nanoparticles for efficient photocatalytic degradation of Rhodamine B. *ChemistrySelect* **2021**, *6*, 5356–5365.
106. Shahsavandi F, Amirjani A, Reza Madaah Hosseini H. Plasmon-enhanced photocatalytic activity in the visible range using AgNPs/polydopamine/graphitic carbon nitride nanocomposite. *Appl. Surf. Sci.* **2022**, *585*, 152728.
107. Meng F, Qin Y, Lu J, Lin X, Meng M, Sun G, et al. Biomimetic design and synthesis of visible-light-driven g-C_3N_4 nanotube @polydopamine/NiCo-layered double hydroxides composite photocatalysts for improved photocatalytic hydrogen evolution activity. *J. Colloid Interface Sci.* **2021**, *584*, 464–473.
108. Yang Y, Lai Q, Mahmud S, Lu J, Zhang G, Huang Z, et al. Potocatalytic antifouling membrane with dense nano-TiO_2 coating for efficient oil-in-water emulsion separation and self-cleaning. *J. Membr. Sci.* **2022**, *645*, 120204.
109. Sun X-H, Chen S-H, Guo Q-Z, Shen Z-C, Wu J, Du Z-X. Convenient recycling and efficient photocatalytic degradation of disinfection by-products by in-situ growth MOF on PET. *Sep. Purif. Technol.* **2023**, *324*, 124506.
110. Zheng H, Meng X, Yang Y, Chen J, Huo S. Bifunctional photocatalytic nanofiltration membranes with immobilized $BaTiO_3$/$Ti_3C_2T_x$ catalysts for the simultaneous separation and degradation of azo compounds. *J. Environ. Chem. Eng.* **2023**, *11*, 110064.
111. Sun A, Zhan Y, Chen X, Jia H, Zhu F, Zhao C, et al. Design of photocatalytic self-cleaning poly (arylene ether nitrile)/nitrogen-doped $Bi_2O_2CO_3$ composite membrane for emulsified oily wastewater purification. *J. Environ. Chem. Eng.* **2023**, *11*, 110810.
112. Hu Y, Zhao P, Liu H, Yi X, Song W, Wang X. Photocatalytic thin film composite forward osmosis membrane for mitigating organic fouling in active layer facing draw solution mode. *Chin. Chem. Lett.* **2023**, *34*, 107931.
113. Liu Y, Liao M, Gan D, Chen M, Ma L, Yang B, et al. Photocatalytic RGO membrane with carbon nitride nanotube intercalation for enhanced wastewater purification. *Colloids Surf. A* **2023**, *663*, 131080.
114. Ren S, Guo N, Li J, Wang Y. Integration of antibacterial and photocatalysis onto polyethersulfone membrane for fouling mitigation and contaminant degradation. *J. Environ. Chem. Eng.* **2023**, *11*, 110401.

115. Govardhanan B, GokulaKrishnan SA, Arthanareeswaran G, Ashok M, Chen Y-S, Taweepreda W. Photocatalytic bio-inspired PDA-RGO/g-CN nanocomposite incorporated PES membrane for removal of environmental antibiotic pollutants. *J. Chem. Technol. Biotechnol.* **2024**, *99*, 1401–1413.
116. da Silva AFV, Della Rocca DG, Moreira RFPM, Oliveira JV, Ambrosi A, Di Luccio M. Synergistic effects of PVDF membrane surface functionalization with polydopamine and titanium dioxide for enhanced oil/water separation and photocatalytic behavior. *J. Environ. Chem. Eng.* **2024**, *12*, 111854.
117. Ren H-T, Li D-S, Jing M-Z, Li T-T, Lou C-W, Lin J-H. Fabrication of sandwich structure membrane and its performance for photocatalytic reduction of Cr(VI). *Cellulose* **2023**, *30*, 3165–3183.
118. Li R, Xiao G, Chen C, Chen C, Hu X, Li Y, et al. Self-assembly graphene oxide membrane embedded with CPU@PAA@TiO_2 for enhancing the dyes separation and photocatalytic self-cleaning performance. *J. Membr. Sci.* **2023**, *683*, 121816.
119. Zhang H, Zhang J, Luo J, Wan Y. A novel paradigm of photocatalytic cleaning for membrane fouling removal. *J. Membr. Sci.* **2022**, *641*, 119859.
120. Le TMH, Wang R, Sairiam S. Self-protecting PVDF-PDA-TiO_2 membranes towards highly efficient and prolonged dye wastewater treatment by photocatalytic membranes. *J. Membr. Sci.* **2023**, *683*, 121789.
121. Liu L, Wang D, Huang J, Huang Z, Zhang Y, Li L. Multicomponent composite membrane with three-phase interface heterostructure as photocatalyst for organic dye removal. *ACS Omega* **2022**, *7*, 17128–17143.
122. Sui S, Quan H, Yang X, Dong X, Ji Y, Liu C, et al. Multifunctional modified polyurethane sponge for recovery of oil spills and photocatalytic degradation. *Compos. Part B Eng.* **2024**, *271*, 111176.
123. Zheng L, Zhong K, Huang X, Qian X. Cellulose fibers/polydopamine/zinc sulfide composite paper: Predoping in situ fabrication for biphase interface photocatalytic hydrogen production from water. *Cellulose* **2024**, *31*, 2523–2540.
124. Peng L, Wang H, Li G, Zhang W, Liang Z, An T. Photocatalytic inactivation of airborne bacteria onto g-C_3N_4/TiO_2/Ni-polydopamine/Ni bifunctional coupling filter with non-size dependent capture effect. *Appl. Catal. B* **2023**, *329*, 122580.
125. Yuan M, Xue J, Li J, Ma S, Wang M. PCN-222/Ag_2O-Ag p-n heterojunction modified fabric as recyclable photocatalytic platform for boosting bacteria inactivation and organic pollutant degradation. *Colloids Surf. A* **2023**, *656*, 130474.
126. Wan J, Li H, Xu L, Yan J, Liao Y, Wang X. PDA/PEI-induced in-situ growth of a lotus leaf-like TiO_2 nanoparticle film on N-halamine cotton fabric for photocatalytic, self-cleaning and efficient antibacterial performance. *Cellulose* **2023**, *30*, 3953–3972.
127. Zhao CH, Zhang YP, Wan L, Chen XX, Yuan P, Qu LB. Versatile application of TiO_2@PDA modified filter paper for oily wastewater treatment. *Molecules* **2023**, *28*, 7903.
128. Cui Z, Marcelle SSA, Zhao M, Wu J, Liu X, Si J, et al. Thermoplastic polyurethane/titania/polydopamine (TPU/TiO_2/PDA) 3-D porous composite foam with outstanding oil/water separation performance and photocatalytic dye degradation. *Adv. Compos. Hybrid Mater.* **2022**, *5*, 2801–2816.
129. Liu R, Dai L, Si C-L. Mussel-inspired cellulose-based nanocomposite fibers for adsorption and photocatalytic degradation. *ACS Sustain. Chem. Eng.* **2018**, *6*, 15756–15763.
130. Zou Y, Wang Z, Chen Z, Zhang Q-P, Zhang Q, Tian Y, et al. Synthetic melanin hybrid patchy nanoparticle photocatalysts. *J. Phys. Chem. C* **2019**, *123*, 5345–5352.
131. Zango ZU, Jumbri K, Sambudi N, Ramli A, Abu Bakar N, Saad, B, et al. A critical review on metal-organic frameworks and their composites as advanced materials for adsorption and photocatalytic degradation of emerging organic pollutants from wastewater. *Polymers* **2020**, *12*, 2648.
132. Nekouei F, Wang T, Keshtpour F, Liu Y, Li H, Nekouei S. Effective redox reaction in a three-body smart photocatalyst through multi-interface modulation of organic semiconductor junctioned with metal and inorganic semiconductor. *Appl. Catal. B Environ. Energ.* **2024**, *351*, 123974.
133. Aguilar-Ferrer D, Vasileiadis T, Iatsunskyi I, Ziółek M, Żebrowska K, Ivashchenko O, et al. Understanding the photothermal and photocatalytic mechanism of polydopamine coated gold nanorods. *Adv. Funct. Mater.* **2023**, *33*, 2304208.
134. Zhang Z, Zhang N, Liu Y, Fang Q, Xi J, Xiao Y, et al. Efficient degradation of organic dyes and reduced Cr(VI) in environmental water purification by in-situ deposition of silver nanoparticles on polydopamine-modified M-ATP/PCN. *Catal. Commun.* **2022**, *172*, 106528.
135. Lu X, Gao Z, Wang G, Chen S, Gu Y, Yan B, et al. Mussel-inspired PDA/Ag nanocomposite catalyst for highly-efficient Cr(vi) removal via visible light-induced reduction and absorption. *New J. Chem.* **2023**, *47*, 9066–9076.
136. Xing C, Ma M, Chang J, Ji Z, Wang P, Sun L, et al. Polyoxometalate anchored zinc oxide nanocomposite as a highly effective photocatalyst and bactericide for wastewater decontamination. *Chem. Eng. J.* **2023**, *464*, 142632.
137. Ding T, Zhang L, Han J, Zhou J, Han Y. Photo-responded antibacterial therapy of reinfection in percutaneous implants by nanostructured bio-heterojunction. *Small* **2023**, *19*, e2206265.
138. Zhang F, Wu C, Zhou Z, Wang J, Bao W, Dong L, et al. Blue-light -activated nano-TiO_2@PDA for highly effective and nondestructive tooth whitening. *ACS Biomater. Sci. Eng.* **2018**, *4*, 3072–3077.
139. Huang Q, Chen J, Liu M, Huang H, Zhang X, Wei Y. Polydopamine-based functional materials and their applications in energy, environmental, and catalytic fields: State-of-the-art review. *Chem. Eng. J.* **2020,** *387*, 124019.

140. Teng X, Liu X, Cui Z, Zheng Y, Chen D-f, Li Z, et al. Rapid and highly effective bacteria-killing by polydopamine/IR780@MnO_2–Ti using near-infrared light. *Prog. Nat. Sci- Mater.* **2020**, *30*, 677–685.
141. Dong W, Zhou S-A, Ma Y, Chi D-J, Chen R, Long H-M, et al. N-doped C-coated $MoO_2/ZnIn_2S_4$ heterojunction for efficient photocatalytic hydrogen production. *Rare Met.* **2023**, *42*, 1195–1204.
142. Ma Y, Fang H-X, Chen R, Chen Q, Liu S-J, Zhang K, et al. 2D-MOF/2D-MOF heterojunctions with strong hetero-interface interaction for enhanced photocatalytic hydrogen evolution. *Rare Met.* **2023**, *42*, 3993–4004.
143. Yan Y, Zhou L, Wang H, Song Z, Jing L, Hu J. Photothermal $ReO_2/ReS_2/Zn_2In_2S_5$ heterojunction for enhanced photocatalytic hydrogen evolution. *Sep. Purif. Technol.* **2024**, *346*, 127473.
144. Wang H, Lin Q, Yin L, Yang Y, Qiu Y, Lu C, et al. Biomimetic design of hollow Flower-like g-C_3N_4@PDA organic framework nanospheres for realizing an efficient photoreactivity. *Small* **2019**, *15*, e1900011.
145. Yang F, Wang S, Li Z, Xu Y, Yang W, Yv C, et al. Polydopamine/defective ultrathin mesoporous graphitic carbon nitride nanosheets as Z-scheme organic assembly for robust photothermal-photocatalytic performance. *J. Colloid Interface Sci.* **2022**, *613*, 775–785.
146. Ran J, Jaroniec M, Qiao SZ. Cocatalysts in semiconductor-based photocatalytic CO_2 reduction: Achievements, challenges, and opportunities. *Adv. Mater.* **2018**, *30*, 1704649.
147. Xu S-R, Xiao F-X. Metal halide perovskites quantum dots: Synthesis and modification strategies for solar CO_2 conversion. *Chin. J. Struct. Chem.* **2023**, *42*, 100173.
148. Xu Q-J, Jiang J-W, Wang X-F, Duan L-Y, Guo H. Understanding oxygen vacant hollow structure $CeO_2@In_2O_3$ heterojunction to promote CO_2 reduction. *Rare Met.* **2023**, *42*, 1888–1898.
149. Hayat A, Sohail M, Iqbal W, Taha TA, Alenad AM, Al-Sehemi AG, et al. Molecular engineering optimized carbon nitride photocatalyst for CO_2 reduction to solar fuels. *J. Sci-Adv. Mater. Dev.* **2022**, *7*, 100483.
150. Dimitrijevic NM, Saponjic ZV, Bartels DM, Thurnauer MC, Tiede DM, Rajh T. Revealing the nature of trapping sites in nanocrystalline titanium dioxide by selective surface. *J. Phys. Chem. B* **2003**, *107*, 7368–7375.
151. Meng A, Cheng B, Tan H, Fan J, Su C, Yu J. TiO_2/polydopamine S-scheme heterojunction photocatalyst with enhanced CO_2-reduction selectivity. *Appl. Catal. B Environ.* **2021**, *289*, 120039.
152. Li M, Zhang S, Li L, Han J, Zhu X, Ge Q, et al. Construction of highly active and selective polydopamine modified hollow ZnO/Co_3O_4 p-n heterojunction catalyst for photocatalytic CO_2 reduction. *ACS Sustain. Chem. Eng.* **2020**, *8*, 11465–11476.
153. Hu J, Chen C, Yang H, Yang F, Qu J, Yang X, et al. Tailoring well-ordered, highly crystalline carbon nitride nanoarrays via molecular engineering for efficient photosynthesis of H_2O_2. *Appl. Catal. B Environ.* **2022**, *317*, 121723.
154. Ma J, Peng X, Zhou Z, Yang H, Wu K, Fang Z, et al. Extended conjugation tuning carbon nitride for non-sacrificial H_2O_2 photosynthesis and hypoxic tumor therapy. *Angew. Chem. Int. Ed Engl.* **2022**, *61*, e202210856.
155. Zhao Y, Gao J, Yang Z, Li L, Cui J, Zhang P, et al. Efficient exciton dissociation in ionically interacted methyl viologen and polymeric carbon nitride for superior H_2O_2 photoproduction. *ACS Catal.* **2023**, *13*, 2790–2801.
156. Wang J, Zhao H, Larter SR, Kibria MG, Hu J. One-pot sequential cascade reaction for selective gluconic acid production from cellulose photobiorefining. *Chem. Commun.* **2023**, *59*, 3451–3454.
157. Wei Z, Zhao S, Li W, Zhao X, Chen C, Phillips DL, et al. Artificial photosynthesis of H_2O_2 through reversible photoredox transformation between catechol and o-benzoquinone on polydopamine-coated CdS. *ACS Catal.* **2022**, *12*, 11436–11443.
158. Deng Y, Liu W, Xu R, Gao R, Huang N, Zheng Y, et al. Reduction of superoxide radical intermediate by polydopamine for efficient hydrogen peroxide photosynthesis. *Angew. Chem. Int. Ed Engl.* **2024**, *63*, e202319216.
159. Wei Y, Jiang W, Liu Y, Bai X, Hao D, Ni BJ. Recent advances in photocatalytic nitrogen fixation and beyond. *Nanoscale* **2022**, *14*, 2990–2997.
160. Ziegenbalg D, Zander J, Marschall R. Photocatalytic nitrogen reduction: Challenging materials with reaction engineering. *ChemPhotoChem* **2021**, *5*, 792–807.
161. Wang T, Liu J, Wu P, Feng C, Wang D, Hu H, et al. Direct utilization of air and water as feedstocks in the photo-driven nitrogen reduction reaction over a ternary Z-scheme SiW_9Co_3/PDA/BWO heterojunction. *J. Mater. Chem. A* **2020**, *8*, 16590–16598.
162. Shi J-L, Lang X. Assembling polydopamine on TiO_2 for visible light photocatalytic selective oxidation of sulfides with aerial O_2. *Chem. Eng. J.* **2020**, *392*, 123632.
163. Ghorbani F, Zamanian A, Behnamghader A, Joupari MD. A facile method to synthesize mussel-inspired polydopamine nanospheres as an active template for in situ formation of biomimetic hydroxyapatite. *Mater. Sci. Eng. C* **2019,** *94*, 729–739.
164. Boecker M, Micheel M, Mengele AK, Neumann C, Herberger T, Marchesi D'Alvise T, et al. Rhodium-complex-functionalized and polydopamine-coated CdSe@CdS nanorods for photocatalytic NAD^+ reduction. *ACS Appl. Nano Mater.* **2021**, *4*, 12913–12919.
165. Wang Y-M, Li W-J, Wang M-M, Zhang M, Zhang Z-H. Magnetic MoS_2 efficient heterogeneous photocatalyst for the α-methoxymethylation and aminomethylation of aromatic ketones. *Catal. Sci. Technol.* **2023**, *13*, 665–674.
166. Xu L, Zhang SZ, Li W, Zhang ZH. Visible-light-mediated oxidative amidation of aldehydes by using magnetic CdS quantum dots as a photocatalyst. *Chem. Eur. J.* **2021**, *27*, 5483–5491.